

Figure 2. Ribbon of the novel aligned nanotube solid material produced upon filtering a colloidal suspension of nanotubes in a magnetic field of 25 T. Due to the high degree of organization, the material cleaves along lines parallel to the magnetic field. This material holds great promise for studying, in a bulk assembly, the anisotropic properties of nanotubes.

model reveals that the alignment energy of the nanotubes at 19 T is (28 ± 3) times thermal energy at room temperature.

To study further the properties of aligned nanotubes, we assembled them into a solid layer by filtration in a magnetic field parallel to the filter membrane surface. Upon drying, the resulting film could be peeled off the filter membrane. It cleaved readily into long ribbons with edges parallel to the magnetic field direction (Figure 2), demonstrating that it consists of long ropes of nanotubes that are well-oriented parallel to the field. Ongoing experiments are exploring the electronic and optical properties of this novel material. It may even be capable of acting as a seed crystal for the growth of continuous nanotube cables and fibers.

Acknowledgements: This work was supported by the Office of Naval Research (#N00014-99-1-0246), the National Aeronautics and Space Administration (#NCC 9-77), and the Welch Foundation.

- ¹ Thess, A., *et al.*, *Science*, **273**, 483 (1996).
- ² Lu, J.-P., *Phys. Rev. Lett.*, **74**, 1123 (1995).

MAGNETIC RESONANCE TECHNIQUES

Solid State NMR Studies in Polypropylenes

Alamo, R.G., FAMU-FSU College of Engineering,
Chemical Engineering

Solid State NMR studies of polypropylenes have been performed within two ongoing research programs in our laboratory.

The first program focuses in understanding the partitioning of the defects of the polypropylene molecule among the different phases of the lamellar crystallite. Homo-polypropylenes and different types of random propylene copolymers have been studied and resonances associated with the defects in the crystallite regions have been identified directly by CP MAS ¹³C NMR as well as theoretically by quantum chemical computations. This work has been carried out in collaboration with Dr. D. VanderHart of the National Institute of Standards and Technology (NIST). Two main papers have been submitted to *Macromolecules* and the work has been presented in different meetings of the American Chemical and Physical Societies.

A second program is directed to understand the conformational and dynamic properties that cause profound melting kinetics in the fusion of polypropylene crystals. This work is part of Ms. W.T. Huang's Ph.D. thesis. Spin lattice relaxation (T_{1H}) in the interlamellar amorphous region are measured aiming to understand relaxation and conformational properties of this region. These studies will be completed during the 2000 Spring

semester. Polypropylenes with different defects contents will be crystallized for different lengths of time and the T_{1H} will be measured. The results will determine if melting kinetics is a consequence of entropic change in interlamellar constrained regions during crystallization. Ms. Huang is expected to defend her Ph.D. in the Fall of 2000.

Development of Large Volume High Frequency RF Coils

- Beck, B., University of Florida Brain Institute (UFBI),
NHMFL
Brooker, R., Univ. of South Florida
Blackband, S.J., UFBI/UF Center for Structural Biology/
NHMFL
Fitzsimmons, J., UFBI/UF, Radiology
Duensing, R., UFBI/UF, Radiology
Peterson, D., UFBI/UF, Radiology

Traditional design techniques used at lower field strengths begin to break down on high field instruments, requiring a new perspective at these higher frequencies. Recent techniques appearing in the literature involve the use of resonant cavities with Vaughans's TEM resonator the most widely applied.¹ The purpose of this work is to explore and simplify one specific type of cavity, the reentrant cavity, and as a proof of concept, construct and image with this simplified design. This work has been accepted by the next ISMRM meeting.²

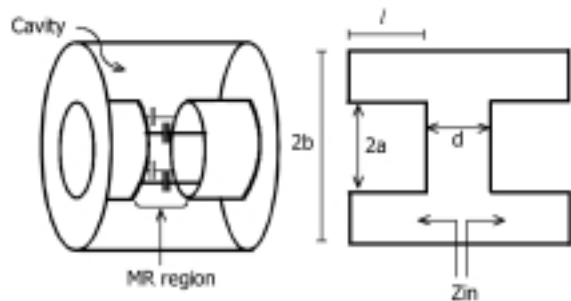


Figure 1. Left: ReCav coil; Right: cross sectional equivalent.

A coaxial reentrant cavity, or ReCav coil (see Figure 1), was made for use on a 4.7 T Bruker Avance system and compared with a conventional birdcage coil. The ReCav has a much higher unloaded Q than the birdcage, but ends up with equivalent Q in the loaded case. Q damping is much greater for the ReCav. The SNR results indicate equivalent operation for the two coils. The performance equivalence of the ReCav coil and the birdcage is very encouraging because one would expect a small birdcage at 200 MHz to perform very well. As the frequencies get higher and the coil sizes approach significant portions of a wavelength, however, the ReCav efficiency may be better than the birdcage because of its ability to contain the electromagnetic fields. Also, in comparison to other designs in the literature, the ReCav coil is very simple to construct and control. We have begun investigating larger ReCav designs at 500 MHz in expectation of delivery of a 40 cm clear bore, 11.7 T Bruker system.

Acknowledgements: This research was supported by the NHMFL and UFBI.

¹ Vaughan, J.T., *et al.*, MRM, 32:206-218, 1994.

² Beck, B., *et al.*, accepted to ISMRM Proceedings 2000.

Hyperpolarized Xenon-129 NMR Studies of Xenon-Protein Interactions in the Solution and Lyophilized State **IHRP**

Bowers, C.R., UF, Chemistry/NHMFL

Storhaug, V., UF, Chemistry

Webster, E., UF, Chemistry

Bharatam, J., UF, Chemistry

Cottone, A., UF, Chemistry

Gianna, R., UF, Chemistry

Gaffney, B.J., FSU, Biology

The generation of hyperpolarized ^{129}Xe by spin exchange optical pumping affords an enhancement by 3-4 orders of magnitude of its NMR signal. As a result, it is possible to observe Xe directly bound to the surface of micromole quantities of lyophilized protein. In this work, an exploratory study of the binding interactions of xenon to the surface of several different proteins in the solution and solid states was studied using both conventional and hyperpolarized ^{129}Xe NMR. The

highly sensitive nature of the ^{129}Xe lineshape and chemical shift are used as indicators for the conditions most likely to yield maximal dipolar contact between ^{129}Xe nuclei and nuclear spins situated on the protein. This is an intermediate step toward achieving the ultimate goal of NMR enhancement of the binding site nuclei by polarization transfer from hyperpolarized ^{129}Xe . The hyperpolarized ^{129}Xe spectra resulting from exposure of four different proteins in the lyophilized, powdered form have been examined for evidence of binding. Each of the proteins, namely, metmyoglobin, methemoglobin, hen egg white lysozyme, and soybean lipoxygenase, yielded a distinctly different NMR lineshape. With the exception of lysozyme, the proteins all possess a paramagnetic iron center that can be expected to rapidly relax the ^{129}Xe and produce a net shift in its resonance position if the noble gas atom occupies specific binding sites near the iron. At temperatures from 223 to 183 K, NMR signals were observed in the 0 to 40 ppm chemical shift range, relative to Xe in the gas phase. The signals broadened and shifted downfield as the temperature was reduced, indicating that Xe is exchanging between the gas phase and internal or external binding sites of the proteins. Additionally, conventional ^{129}Xe NMR studies of met-myoglobin and lipoxygenase in the solution state are presented. The temperature dependence of the chemical shift and lineshape indicate exchange of Xe between adsorption sites on lipoxygenase with Xe in the solvent on the slow to intermediate exchange time-scale. The NMR results are compared with N_2 , Xe, and CH_4 gas adsorption isotherms. It is found that lipoxygenase is unique among the proteins studied in possessing a relatively high affinity for gas molecules, and in addition, demonstrates the most clearly resolved ^{129}Xe NMR peak due to absorption by the lyophilized protein.

Development of Novel Multi-Layer Transverse Gradient Coils

Bowtell, R., Univ. of Nottingham, England, Physics

Crozier, S., Univ. of Queensland, Australia, MR Centre

Beck, B., Univ. of Florida Brain Institute (UFBI)

Blackband, S.J., UFBI/UF, Neuroscience/NHMFL

Gradient strength is an important criteria in NMR in general, and for MRI studies in a variety of systems. It is important that the NMR signal be dephased/encoded in a time period that is short compared to the NMR characteristic that we wish to measure. For example, sufficient diffusion weighting in MR is critically dependant on the gradient strength so that the echo time is as small as possible. In this way the SNR is maximized and diffusion times are reduced.

The gradient strength achievable with a wire coil array is dependant on the current that the coil can support without destruction. At small physical sizes, such as those employed in high resolution of so-called MR microscopy, it becomes physically impractical to increase the wire winding density. To alleviate this limitation, Dr. Bowtell and co-workers at

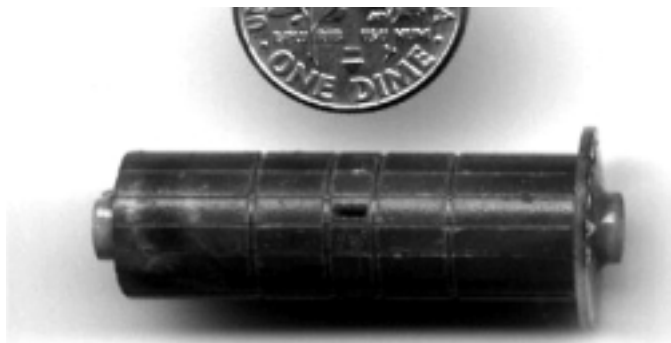


Figure 1. Photo of the multilayer gradient coil.

Nottingham University have pioneered the development of multilayer gradient coil arrays, so far building an axial coil of this design. An axial coil encodes just one spatial direction (z), and so transverse coils (x,y) are also required, but more difficult to fabricate. In this collaboration, a multilayer transverse gradient coil array was constructed by hand and demonstrated the expected electrical characteristics. In collaboration with Dr. Crozier in Australia, a similar coil was constructed by machine and tested with NMR techniques.¹ The coil again demonstrated the expected improvements in performance (manuscript in preparation) and is shown in the figure. The challenge now is to construct a three axis gradient set of this design.

Acknowledgements: This research was supported by NIH and UFBI.

¹ Bowtell, R., *et al.*, ISMRM 7th Annual Meeting, (1999).

Multifrequency Quasi-Optical EMR Spectrometer at NHMFL **IHRP**

Brunel, L.-C., NHMFL

Budil, D.E., Northeastern Univ., Chemistry

Krzystek, J., NHMFL

Saylor, C.A., NHMFL

Sienkiewicz, A., Institute of Physics, Polish Academy of Science, Warsaw, Poland

Smith, G.M., St. Andrews Univ., Fife, Scotland, Physics and Astronomy

Van Tol, J., NHMFL

Wylde, R., Thomas Keating Ltd., West Sussex, England

The high field EMR spectrometer in operation at NHMFL since 1995 has been vastly successful in solving a variety of scientific problems ranging from solid state physics to chemistry to biochemistry.¹ At the same time it had certain drawbacks such as (1) sensitivity insufficient to study dilute spin systems as often encountered in biochemistry, and (2) lack of phase control that resulted in random absorption/dispersion ratios in the recorded spectra. In order to account for those deficiencies, a new

EMR spectrometer based on the existing 17 T superconducting magnet was designed and developed in cooperation Dr. D. Budil, Northeastern University, and with Thomas Keating Ltd., a high-technology company based in Great Britain.

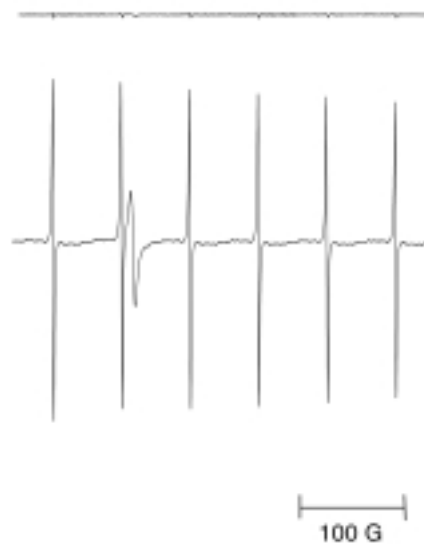


Figure 1. Sensitivity comparison between the old transmission (top) and new quasi-optical (bottom) EMR spectrometers using the same standard sample (MnO/MgO). The spectra were taken at 220 GHz and 293 K, and are normalized for noise amplitude.

The new spectrometer uses quasi-optical (QO) principles of propagating mm and sub-mm waves as a Gaussian beam in open space.² A set of reflecting flat mirrors, semi-reflecting/polarizing tungsten wire grids and focusing off-axis elliptical mirrors elements combined with a ferrite-based Faraday rotator is used to emulate a balanced bridge configuration with a reference arm. After being processed through the bridge, the mm or sub-mm beam is directed into a low-loss corrugated cylindrical waveguide capable of propagating the polarization-preserving HE₁₁ hybrid mode. The detection scheme is based on the induction principle.³ The cross-polar EMR signal is led back from the sample space through the corrugated waveguide and separated from the incident beam using polarizing grids. It is then combined with the local oscillator beam (which passes through a phase shifter) and detected in a SbIn liquid helium-cooled mixer. The spectrometer thus operates in a homodyne mode.

The QO spectrometer preserves what was the most unique and useful characteristics of the previous instrument, namely its multifrequency capability, covering the 180 to 380 GHz frequency range. This was made possible by constructing two different corrugated probes, and employing two SbIn mixers, each optimized for a different frequency range (180 to 250 GHz and 280 to 380 GHz, respectively). Preliminary measurements have shown that the new spectrometer is characterized by an absolute sensitivity on the order of 5×10^{10} spins/Gauss at room temperature. That is approximately two orders of magnitude better than the previous arrangement, and on par with a modern commercial X-band spectrometer. At the same time there is full control of the EMR signal phase thanks to the homodyne

detection. Future developments will include a Fabry-Pérot resonator to further increase the sensitivity as well as to make it possible to measure aqueous samples at room temperature.

- ¹ Hassan, A.K., *et al.*, *J. Magn. Reson.*, **142**, 300 (2000).
- ² Goldsmith, P.F., *Quasioptical Systems* (Piscataway: IEEE Press, 1998).
- ³ Teaney, D.T., *et al.*, *Rev. Sci. Instr.*, **32**, 721 (1961).

K₃CrO₈ In K₃NbO₈ as a Proposed Standard for G-Factor, Spin Concentration, and Field Calibration in High Field EPR Spectroscopy

Cage, B., NHMFL/FSU, Chemistry
 Weekley, A., FSU, Chemistry
 Brunel, L.-C., NHMFL/FSU, Physics
 Dalal, N.S., NHMFL/FSU, Chemistry

This study was motivated by our need to develop a versatile electron paramagnetic resonance (EPR) standard that should have the following characteristics¹:

- (a) narrow EPR lines, which is a prerequisite for achieving high accuracy in the g-value measurement (i.e. 0.00005);
- (b) its EPR spectrum should be as simple as possible, preferably an S = 1/2, I = 0 system;
- (c) obtainable in pure, reproducible form;
- (d) its peaks be close to, but not overlapping and obscuring sample's peaks;
- (e) capable of providing both g-value and field calibration;
- (f) free from phase transitions in order to be a good standard for variable temperature or field dependent work;
- (g) a good intensity standard by displaying Curie like or predictable temperature dependence;
- (h) free of any significant temperature or field dependent linewidths.

The results suggest that K₃CrO₈ essentially meets all of these criteria. For 0.5% K₃CrO₈ in niobate at room temperature, the H_{pp} is 1.5 G at 9.5 GHz (0.33 T), 2.8 G at 110 GHz (3.9 T) and only about 3.3 G at the highest frequency investigated, 330 GHz (11.8 T). In contrast to DPPH and Mn(II) in MgO, the linewidth is essentially temperature independent down to 5 K, with the intensity basically following a standard Boltzmann behavior down to at least 5 K. The spin count of the dilute powder can be calibrated against a known amount of pure K₃CrO₈ using EPR spectroscopy. Therefore, as an intensity standard this compound has distinct advantages over both Mn(II) in MgO and DPPH whose spin concentration is not easy to determine because of the difficulty in obtaining preparatory details, and persistent solvent contamination, respectively. Finally, dilute K₃CrO₈ provides an easy field linearity calibration using the hyperfine splitting: A_{iso} = 20.02 ± 0.05 G when diluted into basic aqueous solution; or diluted into a niobate solid solution gives A_⊥ = 11.49 ± 0.05 G, and A_{||} = 39.55 ± 0.08 G (after second order correction). Table 1 lists the various advantages and disadvantages of 0.5% K₃CrO₈ in K₃NbO₈,

versus the other standards in use, DPPH, Mn(II) in MgO, and ruby, from which it can be noted that K₃CrO₈ has many advantages over the other three.

Table 1. Comparison of various EPR standards.

	0.5% K ₃ CrO ₈ /K ₃ NbO ₈	Mn(II) in MgO	DPPH	Ruby
Concentration standard purity	Absolute spin measurements possible. Easily synthesized in pure form.	Difficult Difficult high temperature synthesis.	Difficult Solvent and sample dependent.	Usable Difficult synthesis.
g-value precision	±0.00005 Good for g < 2 and also good for g = 2.	±0.00005 May overlap g = 2 signals, second order effects.	±0.0002 May overlap g=2 signals, and lineshape is sample dependent.	±0.0006 Broad lines.
Field linearity	Possible via hyperfine. Also possible via two g-values.	Second order hyperfine complications.	No	Not fully investigated.
Temperature Dependence	Simple basically Curie like S=1/2 behavior. Lineshape, hyperfine, and g-values are essentially constant to 5 K.	Significant lineshape changes.	Phase transition at 30 K, significant line broadening.	Complicated S = 3/2 behavior, only investigated to 77 K at high field.

¹ Cage, B., *et al.*, *Anal. Chem.*, **71**, 1951-7 (1999).

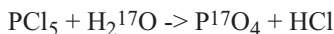
¹⁷O High Resolution Solid State NMR Measurements on Ferroelectrics at Fields Up to 25 T IHRP

Dalal, N.S., FSU, Chemistry/NHMFL
 Giese, M.W., FSU, Chemistry/NHMFL
 Pierce, K.L., FSU, Chemistry/NHMFL
 Fu, R., NHMFL
 Gan, Z., NHMFL

Many electro-optic materials are either metal oxides or contain oxygen atoms at important sites so that oxygen NMR should be an excellent probe for obtaining a detailed understanding of the structure-property relationships of such materials. The present study was undertaken with a view of developing methodologies for obtaining high-resolution ¹⁷O NMR spectra from oxygen-containing solids. While the significance of such a development is well recognized, earlier efforts to obtain high resolution NMR spectra from ¹⁷O have been hampered by several factors: (a) its very low natural abundance (0.038%), hence poor detection limits; and (b) its large nuclear spin, I = 5/2 that leads to extensive quadrupolar splittings and/or broadenings, hence poor resolution. Our approach to solve these problems is to utilize the highest possible Zeeman field (B₀), because the quadrupolar broadening of the "central" transition for odd-half nuclei decreases as 1/B₀, and also because the detection sensitivity scales with the increase in B₀.

In this study we prepared single crystals of ¹⁷O-labeled ferroelectric phosphates like KH₂PO₄ (KDP), and antiferroelectric materials NH₄H₂PO₄ (ADP) and squaric acid

(H₂C₄O₄). The ¹⁷O labeling of the PO₄ moieties, according to this reaction:



and the C-O oxygen was accomplished by isotopic exchange, and verified by mass spectrometry. Figure 1 shows ¹⁷O MAS spectra for ADP at ambient temperature 295 K recorded on the 833 MHz. The spectra at the higher field show the expected increase in sensitivity and resolution. These data thus demonstrate that very high-resolution ¹⁷O spectra are obtainable at fields up to 24 T, which provide a new method for probing the mechanism of ferroelectric and antiferroelectric transitions in a wide variety of solids.

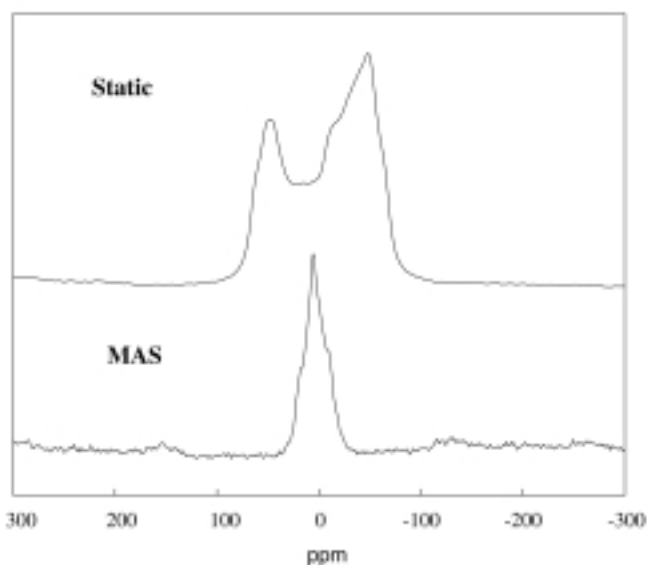


Figure 1. ¹⁷O spectra recorded on the 833 MHz NMR spectrometer at ambient temperature 295 K.

Digital Quadrature Heterodyne Detection for High Resolution Fourier Transform Ion Cyclotron Resonance Mass Spectrometry

Drader, J.J., NHMFL

Shi, S.D.-H., FSU, Chemistry

Hendrickson, C.L., NHMFL

Marshall, A.G., NHMFL/FSU, Chemistry

Blakney, G.T., Univ. of Texas, Chemistry

Laude, D.A., Univ. of Texas, Chemistry

The pursuit of ever higher mass resolving power in Fourier transform ion cyclotron resonance mass spectrometry (FT-ICR MS) has driven a demand for higher magnetic field strength and longer time-domain ICR signal lifetime, with proportionate increase in data set size in direct-mode detection. Heterodyne-mode detection thus becomes increasingly important for achieving ultrahigh mass resolution from a fixed maximum-

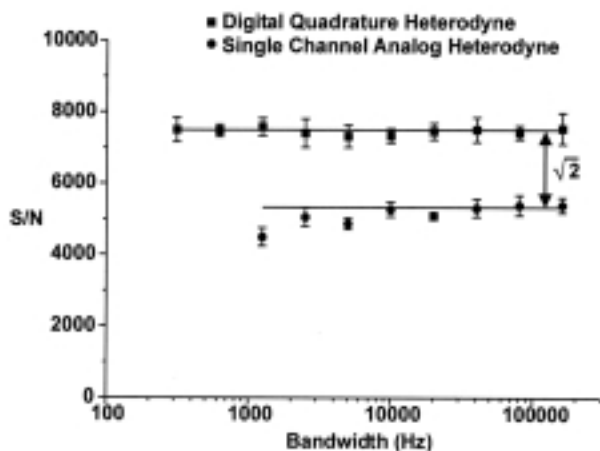


Figure 1. Signal-to-noise ratio vs. spectral bandwidth for digital quadrature heterodyne detection (squares) and single channel analog heterodyne detection (circles).

size data set. Unfortunately, as conventionally performed (i.e., analog single-phase), heterodyne detection reduces the S/N ratio by a factor of $2^{1/2}$ relative to direct-mode detection. Here, we restore the factor of $2^{1/2}$ by use of quadrature heterodyne detection (see figure). In addition, replacement of analog by digital heterodyning eliminates analog circuitry (and its associated noise). Finally, digital filtering of the time-domain discrete ICR signal not only eliminates the need for a bank of analog low-pass filters, but also ensures that the Nyquist bandwidth and filter bandwidth are always matched, for optimal noise reduction. With these features, digital quadrature heterodyne detection becomes the detection method of choice for high-resolution FT-ICR MS.

Acknowledgements: The authors thank Prof. Charles K. Mann for helpful discussions. This work was supported by grants from NSF (CHE-94-13008), Florida State University, and the NHMFL in Tallahassee, FL.

¹ Drader, J.J., *et al.*, *Anal. Chem.*, **71**, 4758-4763 (1999).

NMR Studies of Fluoride-Ion Mobility and Oxygen/Fluorine Ordering in Fluorides and Oxyfluorides

Du, L.-S., State Univ. of New York at Stony Brook, Chemistry

Grey, C.P., SUNY at Stony Brook, Chemistry

Samoson, A., National Institute of Chemical Physics and Biophysics, Tallinn, Estonia

Research in our group has shown that ¹⁹F MAS NMR spectroscopy is a powerful tool for investigating oxygen/fluorine ordering in oxyfluorides.¹ If high resolution ¹⁹F spectra can be obtained, then detailed information concerning the mechanisms of fluoride ions motion and the rates can readily be extracted from the ¹⁹F MAS NMR.² In this report, we show the dramatic

improvements that may be obtained in many of these systems by running solid-state NMR at very high fields (19.5 T) and at high spinning speeds (above 40 kHz).

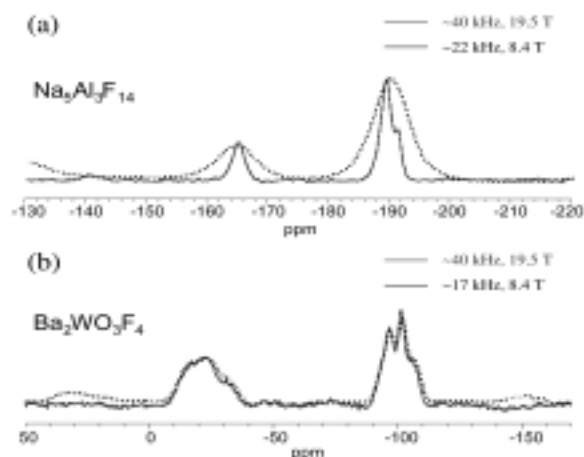


Figure 1. The ^{19}F MAS spectra of $\text{Na}_5\text{Al}_3\text{F}_{14}$, (a), and $\text{Ba}_2\text{WO}_3\text{F}_4$, (b), acquired at 19.5 T and a spinning speed of 40 kHz (solid line) and at 8.4 T and 20 kHz (dashed line).

Figure 1 compares the ^{19}F MAS spectra of chiolite ($\text{Na}_5\text{Al}_3\text{F}_{14}$) (a) and $\text{Ba}_2\text{WO}_3\text{F}_4$ (b) acquired at a field strength of 19.5 T and with a spinning speed of 40 kHz (solid line) and at 8.4 T and a spinning speed of 20 kHz (dashed line). The three crystallographically distinct sites (F1, F2 and F3) could be resolved (for the first time) in the spectrum of chiolite, at high fields. These resonances were assigned to fluorine atoms that bridge two aluminum octahedra (F2; -166 ppm) and four and five coordinate fluorine atoms (F1 and F3, respectively) coordinated to both aluminum and sodium atoms. The high-field spectrum of the isostructural ferroelectric compound $\text{Na}_5\text{W}_3\text{O}_9\text{F}_5$ showed only one broad peak, due to two overlapping resonances. On this basis and from a number of $^{23}\text{Na}/^{19}\text{F}$ CP and HETCOR spectra, obtained at lower fields, we assigned this peak to the F1 and F3 sites. These results indicate that the oxygen atoms are ordered on the bridging sites (now bridging the tungsten octahedra), the residual oxygen atoms ordering on the F3 site. This information could not be obtained from diffraction studies. The spectrum of $\text{Ba}_2\text{WO}_3\text{F}_4$ collected at 19.5 T and at 40 kHz is similar to the spectrum collected at a lower field and spinning speed (Figure 19(b)). Hence, the lineshape of the spectra originate mainly from a distribution of chemical shifts, resulting from the disorder in the anion sites.

^{93}Nb MAS NMR studies have been performed to complement our ^{19}F studies of ordering and mobility in niobium fluorides and oxyfluorides. High field NMR data proved to be essential in deconvoluting the spectra of this high-quadrupole moment nucleus. The ^{93}Nb MAS spectra (solid lines) and simulated results (dashed lines) of K_2NbF_7 and $\text{Cd}(\text{py})_4\text{NbOF}_5$ at 8.4 T and a spinning speed of 20 kHz, (a), and at 19.5 T and 43 kHz, (b), are shown in Figure 2. The center band of the central transition is well separated from the spinning sidebands in the high field spectrum of K_2NbF_7 allowing a quadrupole coupling constant of 35 MHz to be extracted from the high field spectrum; this was

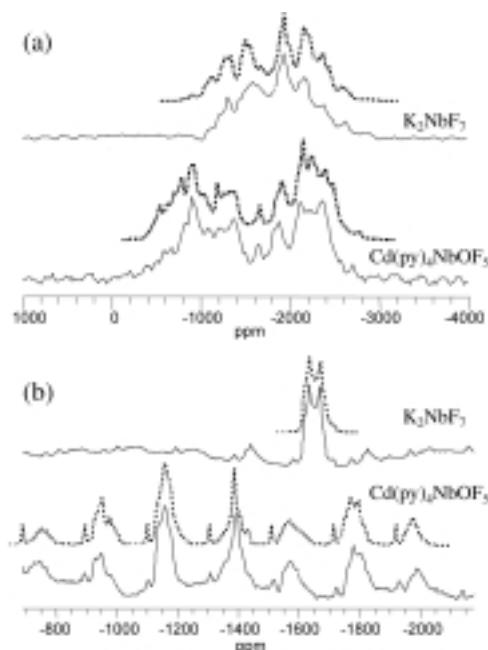


Figure 2. The ^{93}Nb MAS spectra (solid line) and simulated results (dashed lines) of K_2NbF_7 and $\text{Cd}(\text{py})_4\text{NbOF}_5$ at 8.4 T and a spinning speed of 20 kHz, (a), and at 19.5 T and 43 kHz, (b).

then used to simulate the low field spectrum (using the program GAMMA³). Surprisingly, the spectrum of $\text{Cdpy}_4\text{NbOF}_5$ at high fields was dominated by the chemical shift anisotropy (CSA). Simulations of this spectrum allowed the relative orientations of the chemical shift and quadrupolar tensors to be extracted and have aided in our investigation of the O/F ordering in this compound.

¹ Du, L.-S., *et al.*, *J. Solid State Chem.*, **140**, 285 (1998).

² Wang, F., *et al.*, *J. Am. Chem. Soc.*, **117**, 6637 (1995).

³ Smith, S.A. *et al.*, *J. Magn. Reson. A*, **106**, 75 (1994).

Technique Development in EPR Spectroscopy

Fajer, P., NHMFL/FSU, Biology and Institute of Molecular Biophysics

Sale, K., NHMFL/FSU, Biology

Sár, C., Univ. of Pecs, Hungary, Institute of Organic and Medicinal Chemistry

Jek, J., Univ. of Pecs, Hungary, Institute of Organic and Medicinal Chemistry

Hideg, K., Univ. of Pecs, Hungary, Institute of Organic and Medicinal Chemistry

Sienkiewicz, A., National Academy of Sciences, Warsaw, Poland

Our more technological advances were focused on synthesis of new spin labels and development of new EPR resonators.

• Spin labels: (*with K. Hideg*) The development of new spin probes targeting new sites or displaying desired spectral properties is a key in any probe technique. Prof. Hideg and his group at the Univ. of Pecs have developed new spin probes which do not perturb muscle function and which are sensitive to conformational changes previously undetected by the use of commercial spin labels.¹ The latter advantage is due to a novel design of the functional linker that orients the magnetic tensor components perpendicular to the orientation of other labels.

• Microwave resonators: (*with A. Sienkiewicz*) We have designed and tested a new resonator for muscle research. The resonator condenses magnetic field using stacked high dielectric constant ceramics. The high filling factor makes this resonator ideal for studies on small samples like single muscle cells. Low Q of the structure makes it insensitive to mechanical transients arising from perfusion of the cells or mechanical transients used to synchronize the contractile cycle. The resonator is about four times more sensitive than current commercial resonators.^{2,3}

¹ Sar, C.P., *et al.*, *Synthesis*, **6**, 1039-1045 (1999).

² Sienkiewicz, A., *et al.*, *J. Magnetic Resonance*, in press.

³ Fajer, P., *Encyclopedia of Analytical Chemistry*, Wiley, London, in press.

Development of High Frequency Phased Array Rf Coils

Fitzsimmons, J., Univ. of Florida Brain Institute
(UFBI)/UF, Radiology

Duensing, R., UFBI/UF, Radiology

Peterson, D., UFBI/UF, Radiology

Beck, B., NHMFL/UFBI

At high field strengths on large samples (humans) it becomes very difficult if not impractical to construct large body rf coils. It becomes difficult to tune the coil and the rf power requirements become excessive. Consequently most high field studies (above 2 T) on humans have concentrated on the brain where smaller coils can be used. There are substantial benefits for high field imaging outside of the brain, however, and suitable rf coil developments are required.

One option is to use phased array coils as commonly used clinically for signal reception. These coils, however, are normally receive only, requiring a body coil for transmission. A potential solution is to make the phased array coils capable of transmission and reception. At UF the first transceive phased array rf coils were developed at 3 T. A four coil array was developed for imaging the spine. Using this technology the first spinal cord images were obtained on humans at 3 T. These studies are now being extended to other coil types, and we will shortly be funded to develop a transceive phased array head coil.

This technology was further developed by other workers at UF to construct a pelvic phased array coil for prostate studies (see

“Development of Prostate MRI/S Using Transceive Coils at 3 T” elsewhere in this document), and the technology is being used to develop phased array coils for the present 4.7 T/33 cm and upcoming 11.7 T/40 cm animal systems, presently in the prototype stage.

The rf group is also involved in other rf coil developments for a variety of applications indirectly supported by the NHMFL, including birdcage coils for knee imaging at 3 T² and cardiac spectroscopy at 3 T.³

Acknowledgements: This work was supported by the NHMFL and UFBI.

¹ Duensing, *et al.*, ISMRM 6th Annual Meeting (1998).

² Peterson, *et al.*, *Magn Reson Med*, **42**, 215-221 (1999).

³ Bruner, *et al.*, ISMRM 7th Annual Meeting, (1999).

³¹P Isotropic Chemical Shift as a Probe of the Ferroelectric Transition in Ferroelectric RbH₂PO₄ and their Analogs **IHRP**

Fu, R., NHMFL

Dalal, N.S., FSU, Chemistry/NHMFL

The mechanism of the ferro- and antiferroelectric phase transitions observed in the KH₂PO₄ (KDP)-type compounds has been the subject of intense studies over the past decades. One of the important unsolved questions is related to the classification of the transition as either order/disorder or displacive type. As has been shown recently in the ¹³C high resolution NMR study on squaric acid,¹ and emphasized earlier by Blinc² and Mehring³, this question can be answered by careful measurements of the isotropic part of the chemical shift tensor of a probe nucleus. While the anisotropic component of the chemical shift tensor yields information about global symmetry properties, the isotropic part of it is a distinctive measure of electronic structure changes. The results for squaric acid clearly demonstrated that the mechanism of the antiferroelectric transition at 373 K involves a strong displacive component related to charge transfer effects. This conclusion is, however, in contrast to analogous (³¹P NMR) studies on KD₂PO₄ (DKDP) that were interpreted in terms of a purely order/disorder mechanism without any contribution of a displacive component, since no temperature dependences or changes in the isotropic part of the chemical shift could be detected when passing from the paraelectric to the ferroelectric phase, whereas the anisotropic chemical shift correctly reproduces the symmetry lowering that occurs at the phase transition temperature.

Because DKDP is considered to be an ideal model and parent compound of the KDP family, we have reinvestigated the earlier ³¹P NMR data by using an order of magnitude enhancement in spectral resolution. In addition another member of the KDP family, i.e. RbH₂PO₄ (RDP) has been investigated by the same method to generalize our new results. The ³¹P isotropic chemical

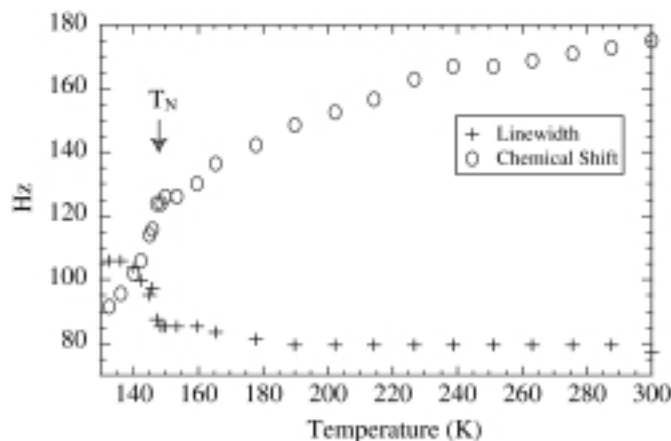


Figure 1. Temperature dependence of the ^{31}P chemical shifts and linewidth of RDP. At $T_N = 148$ K, both the chemical shifts and the linewidth are changed.

shift is found to exhibit a clear break at the phase transition and a pronounced temperature dependence well above the phase transition temperature T_C , with additional changes below it, thus providing new evidence that electronic instabilities are of major importance in these systems. The higher resolution data are interpreted within a model where the cooperative ordering arises through the modifications of potential of the O...H-O bond via charge transfer processes, revealing new aspects about the role of displacive forces, as confirmed by our theoretical analysis. The new aspects of the phase transition dynamics in H-bonded systems could be important in interpreting and understanding other systems like e.g. biomolecules, where hydrogen bonds are commonly observed.

A similar study of $\text{NH}_4\text{H}_2\text{PO}_4$ (ADP) is in progress that will open up a new window on the proton glasses.

- 1 Dalal, N.S., *et al.*, Phys. Rev. Lett., **81**, 5924, (1998).
- 2 Blinc, R., *et al.*, Phys. Rev. Lett., **38**, 92 (1977).
- 3 Mehring, M., *et al.*, Phys. Rev. Lett., **47**, 92 (1981)

Homonuclear Dipolar Recoupling Under Fast MAS by Simultaneous Frequency and Amplitude Modulation

Fu, R., NHMFL

Recently we have been using the simultaneous frequency and amplitude modulation (SFAM)¹ pulse sequence to recouple homonuclear dipolar interaction in the presence of fast MAS. The idea behind SFAM is to introduce time dependence modulation into dipolar interaction using continuous rf irradiation to interfere with MAS such that the dipolar interaction is not averaged by MAS. In the past several years, many experimental techniques have been developed to recover homonuclear dipolar interactions under MAS, so as to obtain

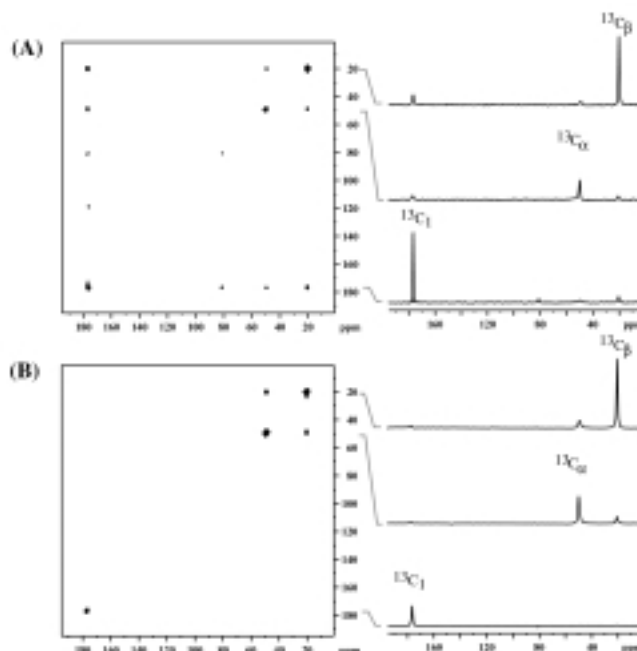


Figure 1. Phase sensitive 2D ^{13}C CPMAS homonuclear correlation spectra of triply-labeled ^{13}C alanine recorded on a Bruker DMX 300. The sample spinning speed was adjusted to 7.2 kHz to avoid rotational resonance effect. The rotor-synchronized 180° pulses² (A) and the SFAM irradiation (B) were applied during the 20.8 ms mixing time. The slices in the right are the phase-sensitive cross sections showing relative intensities of the cross peaks.

distance constraints. A common feature of those techniques is to utilize the flip-flop term of the dipolar interaction without actively interacting with $I_z S_z$ term. We have found the SFAM irradiation to be very efficient for homonuclear dipolar recoupling, owing to the fact that SFAM permits the time-dependence rf irradiation to modulate the entire homonuclear dipolar interaction (both the flip-flop and the $I_z S_z$ terms). This is demonstrated in Figure 1 showing the 2D ^{13}C CPMAS homonuclear correlation spectra. Here the SFAM irradiation with a maximum rf amplitude of 10 kHz was applied to the $^{13}\text{C}_\alpha$ resonance. It is clearly seen that the intensities of the cross peaks between C_α and C_β are more than three times higher in Figure 1B than in Figure 1A. Furthermore, low intensity cross peaks were observed between the C_α and C_1 , and the C_β and C_1 resonances because the C_1 resonance was not affected by the SFAM irradiation. This indicates that SFAM has a potential to isolate a spin pair from a coupling network leading to the determination of the distance between the two spins accurately.

- 1 Fu, R., *et al.*, Chem. Phys. Lett., **272**, 361 (1997).
- 2 Bennett, A.E., *et al.*, J. Chem. Phys., **96**, 8624 (1992).

Inter- and Intramolecular Distance Measurements by Solid State MAS NMR: Determination of Gramicidin A Channel Dimer Structures in Hydrated Phospholipid Bilayers

Fu, R., NHMFL

Cotten, M., NHMFL/FSU, Chemistry

Cross, T.A., NHMFL/FSU, Chemistry

Distance constraints are an important complement to orientational constraints. While a high-resolution monomer structure of the ion channel forming polypeptide, gramicidin A, has been solved with 120 orientational constraints¹ the precise geometry of the dimer interface has not been characterized. As shown in Figure 1, using both ¹³C and ¹⁵N labeled gramicidin A samples in hydrated phospholipid bilayers both inter- and

intramolecular distances have been measured under MAS conditions using the recently developed SFAM technique². By incorporating ¹³C₁-Val₇ and ¹⁵N-Gly₂ labels into gA, an intramonomer dipolar coupling, as weak as 20 Hz, resulted from motionally averaged interactions, was observed confirming the high-resolution structure in this bilayer environment. When incorporating the ¹³C₁-Val₁ and ¹⁵N-Ala₅ labels into gA, only the intermonomer dipolar coupling was observable, allowing for the characterization of the monomer-monomer junction in this lipid environment for the first time. Moreover, magic angle spinning technique yields much higher resolution in solid-state NMR spectra, which allow for the observation of different ¹³C₁ isotropic chemical shifts of the Val₁ residue. This observation suggests the existence of two local conformational states at the monomer-monomer junction that may be associated with channel function.

¹ Ketchum, R.R., *et al.*, *Structure*, **5**, 1655 (1997).

² Fu, R., *et al.*, *Chem. Phys. Lett.*, **272**, 361 (1997).

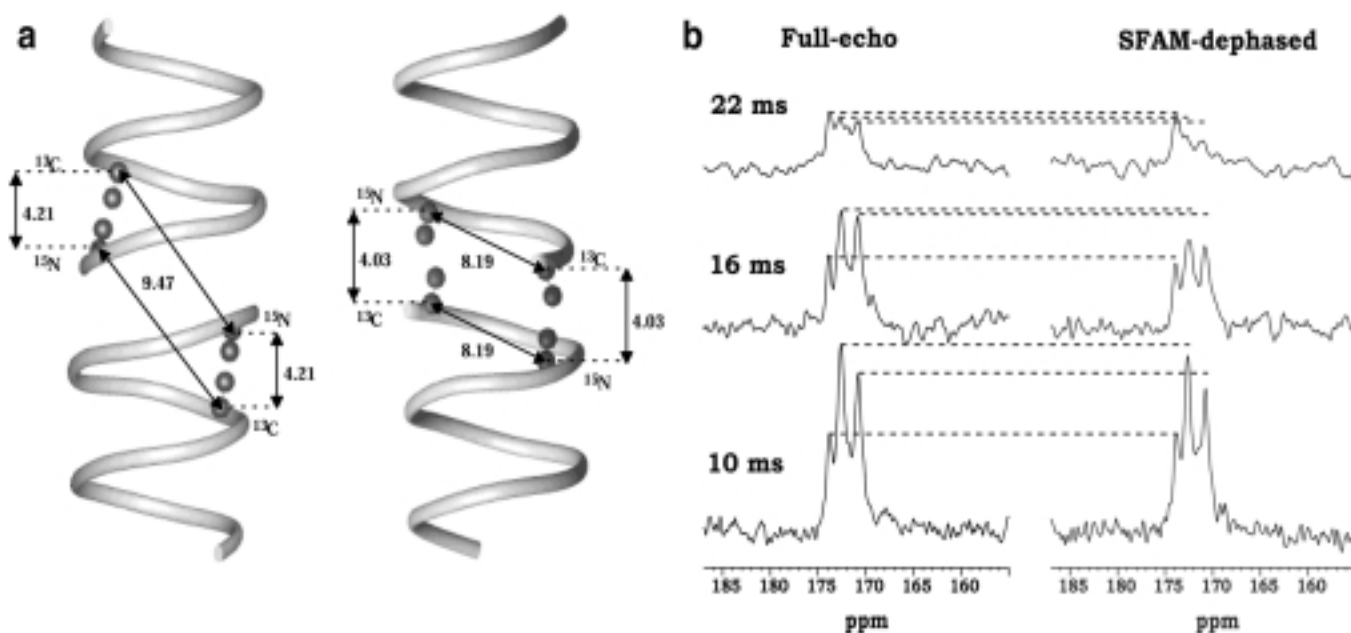


Figure 1. (a) Positions of the specifically labeled ¹³C and ¹⁵N sites in gramicidin A in hydrated phospholipid bilayers. Both ¹³C and ¹⁵N labels are indicated by solid balls at the ribbon. The solid balls, away from the ribbon, but linked to the ¹³C and ¹⁵N labels, represent the oxygen and the hydrogen nuclei, respectively, which are favorably oriented for hydrogen bonding. The distances indicated in the figures are derived from the coordinates of the high-resolution gA structure¹. (Left) ¹³C₁-Val₇, ¹⁵N-Gly₂ gA. For these labels, the distance between the intramonomer ¹³C and ¹⁵N sites is 4.21 Å, while the intermonomer ¹³C and ¹⁵N sites are 9.47 Å apart. (Right) ¹³C₁-Val₁, ¹⁵N-Ala₅ gA. In this case, the separation between the intramonomer ¹³C and ¹⁵N sites is 8.19 Å, while the intermonomer

¹³C and ¹⁵N sites are modeled to be 4.03 Å apart, across the monomer-monomer junction. (b) Sets of SFAM spectra of the ¹³C₁-Val₁, ¹⁵N-Ala₅ gA recorded at 315 K on a Bruker DMX 300 NMR spectrometer with (Right) and without (Left) various SFAM dephasing times. The horizontal dashed lines indicate the intensity differences between the two sets of spectra. Because the peak at 174.0 ppm is not dephased it is therefore assigned to the carbonyl group of the lipids. The remaining two resonances at 171.0 and 172.6 ppm are dephased by the SFAM irradiation on the ¹⁵N spins, indicating a residual dipolar coupling of 38 ± 3 Hz, consistent with the modeled distance.

NMR Study of Proton Storage and Transfer Mechanisms in Amorphous Ruthenium Oxide

Fu, R., NHMFL

Ma, Z.R., NHMFL

Zheng, J.P., FAMU-FSU College of Engineering, Electrical Engineering

A fundamental study of proton storage and transfer mechanisms in ruthenium oxide was conducted by use of nuclear magnetic resonance and electrochemical techniques. The purpose of the study was (1) to establish a comprehensive understanding of the hydrogen transfer and storage mechanisms in ruthenium oxides, (2) to provide a guideline for future improvement of ruthenium oxide, and (3) to provide a foundation for the formulation of analogous materials based on less expensive metallic elements.

The ^1H NMR experiments of amorphous and crystalline ruthenium oxide samples were carried out at a Bruker DMX 300 MHz NMR spectrometer. Narrow ^1H linewidths obtained in amorphous ruthenium oxides clearly demonstrate that the mobility of the ^1H in the amorphous phase is higher than that in the crystalline phase so as to prove that the proton can only be diffused into the amorphous ruthenium oxide.

The ^2H NMR spectra at different temperatures were recorded on a CMX 400 spectrometer on amorphous ruthenium oxide samples in which the protons were replaced by deuterons. It is illustrated that the mobility of the deuteron in amorphous ruthenium oxides is very high until the temperature goes down to $-60\text{ }^\circ\text{C}$ and after this temperature the mobility decreases rapidly.

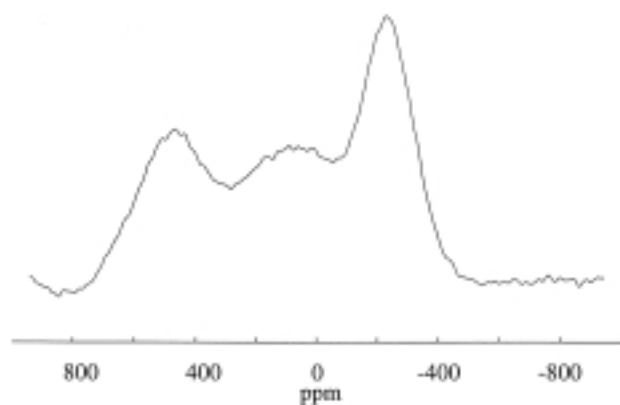


Figure 1. Static state ^{101}Ru NMR spectrum of amorphous $\text{RuO}_2 \cdot x\text{H}_2\text{O}$ ($x=0.76$) obtained at the Keck magnet (25 T) where its Larmor frequency is 55 MHz.

Figure 1 shows a ^{101}Ru NMR spectrum obtained at the Keck magnet (25 T). To our knowledge, this is the first ^{101}Ru NMR measurement on these samples that can only be done at very high field due to its low gamma quadrupolar nucleus. High-resolution MAS measurements on ruthenium oxide will be able to distinguish the Ru valence states at different proton concentrations and different crystalline structures of the ruthenium oxide, which will provide a direct information on the relationship between the proton storage density to the crystalline structure of ruthenium oxides.

Electrochemical property study concluded that high proton storage could be obtained in amorphous ruthenium oxides due to an unexpectedly high degree of proton intercalation. In contrast, for crystalline ruthenium oxides, the proton could only be stored at the surface; therefore, resulting in a lower proton density.

Solid State NMR Applications at Very High Fields: Preliminary Spectra at the 833 MHz

Fu, R., NHMFL

Gan, Z., NHMFL

Dalal, N.S., FSU, Chemistry/NHMFL

Cross, T.A., NHMFL/FSU, Chemistry

Samoson, A., Estonian Academy of Sciences, Estonia

Two unique high field magnets, a 19.6 T (833 MHz) superconducting narrow bore (31.6 mm) and a 25 T (1066 MHz) resistive standard bore, are currently available for solid-state NMR spectroscopy. Some preliminary spectra have been obtained leading to the establishment of collaborations with external users.

Cross polarization (CP) is one of the important techniques in NMR. It enhances the sensitivity of dilute spins such as ^{13}C , ^{15}N through polarization from abundant spins like ^1H . Figure 1 demonstrates a ^{13}C CPMAS spectrum of Adamantane without room temperature shimming using a 2.75 mm double resonance MAS probe. The ^{13}C linewidths obtained were 20 Hz, indicating good field homogeneity across the small sample region.

The NMR observation of low gamma nuclei is difficult because of its inherent low sensitivity and long probe ring down time at low rf frequencies. High magnetic fields not only provide much higher sensitivity but also shorten the probe ring down time. Figure 2 shows a ^{109}Ag MAS spectrum of silver nitrate obtained on the 833 MHz. Silver ions play an important role in ionic conductors. This ^{109}Ag observation has attracted several external users.

For low gamma nuclei, high fields also narrows spectral lines by attenuating the second order quadrupolar effect so as to

High Resolution NMR of Half-Integer Quadrupolar Nuclei Using Satellite Transitions and Magic-Angle Spinning (STMAS)

Gan, Z., NHMFL

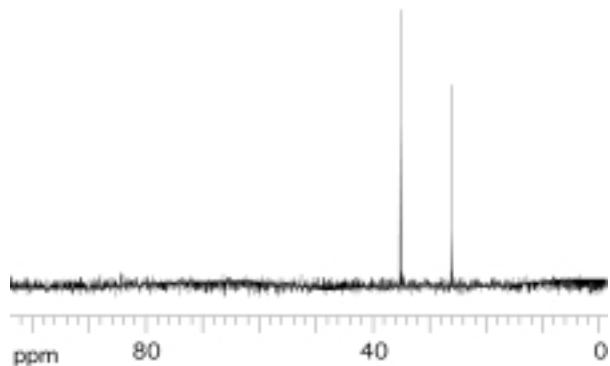


Figure 1. ^{13}C CPMAS spectrum of Adamantane recorded on the 833 MHz using a 2.75 mm double resonance NMR probe. The sample was spinning at 3 kHz. The linewidths obtained were 20 Hz.

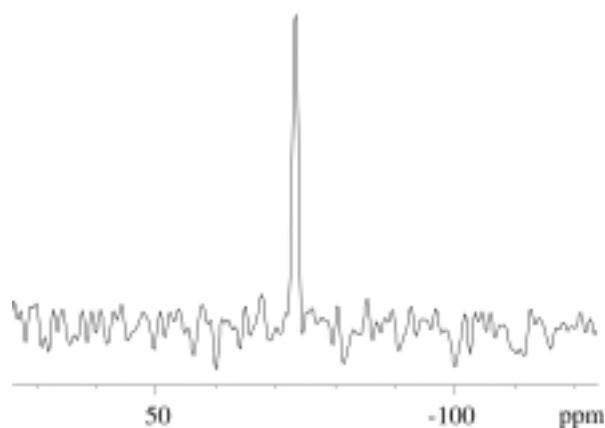


Figure 2. ^{109}Ag MAS spectrum of Silver Nitrate recorded on the 833 MHz. The sample was spinning at 10 kHz. The linewidth was 31 Hz after exponential broadening of 20 Hz. 1024 scans were used to accumulate the signal with a recycle time of 200 s.

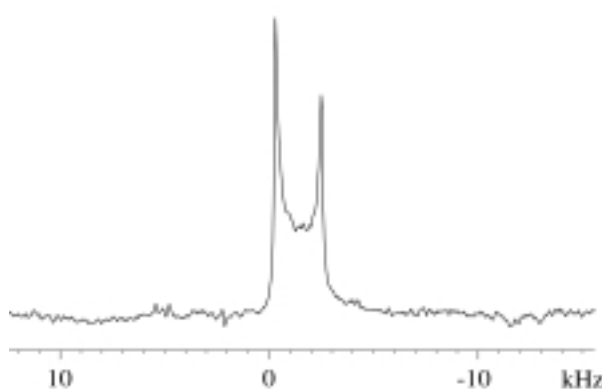


Figure 3. ^{39}K MAS spectrum of KH_2PO_4 recorded on the 833 MHz. The sample was spinning at 16 kHz. 10240 scans were used to accumulate the signal with a recycle time of 2 s.

increase both the spectral sensitivity and resolution. As an example, K is a superionic charge carrier in many photonic crystals such as KDP (KH_2PO_4) and KTP (KTiPO_4). Figure 3 shows a ^{39}K MAS spectrum of KDP. The application to KTP is in progress. It is expected that the results will help us obtain a better understanding of the structure-property relationship for the electro-optical materials, which has not been possible without the availability of the high field systems.

NMR spectroscopy of quadrupolar nuclei such as ^{11}B , ^{17}O , ^{23}Na , ^{27}Al , ^{71}Ga , ^{87}Rb has become an important tool for structural characterization of many important materials such as minerals, ceramics, glasses, semiconductors and catalysts. The NMR line width of quadrupolar nuclei is dominated by the second-order quadrupolar effect that cannot be completely averaged by the conventional magic-angle sample spinning (MAS). The high magnetic fields available at NHMFL can greatly reduce the second-order quadrupolar effect, however, the complete removal of the line broadening relies on techniques such as double rotation (DOR)¹, dynamic-angle spinning (DAS)² and multiple-quantum magic-angle spinning (MQMAS)³. This report describes a new technique based on the satellite transitions and magic-angle spinning (STMAS) that obtains high spectral resolution for quadrupolar nuclei.

Under MAS, the satellite transitions in the manifold of quadrupolar spins are shifted by the second-order quadrupolar effect similar to the central transition. The correlation between the satellite and central transitions averages the remaining high-order line broadening under MAS of the second-order quadrupolar effect. With precise setting of the magic-angle, the

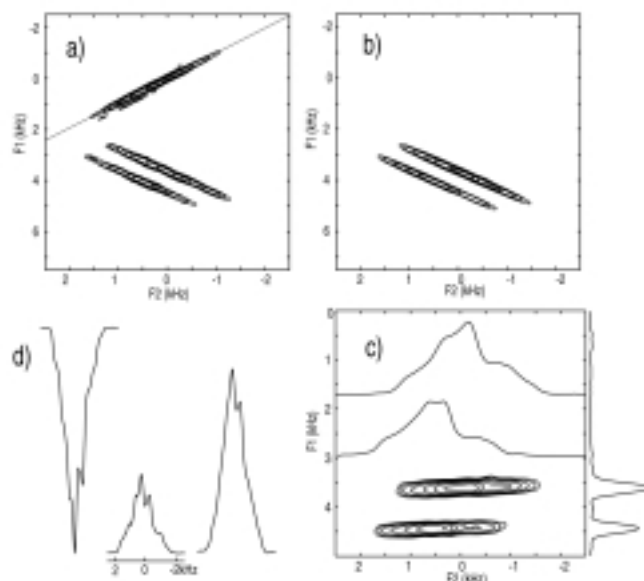


Figure 4. STMAS spectra of a mixture of Na_2SO_4 and $\text{Na}_2\text{C}_2\text{O}_4$ acquired using a three-pulse (a) and a two-pulse (b) sequences. The spectrum in (c) is obtained by a special tilt of (b) and the projection along F1 shows the isotopic shift. The spectra in (d) shows projections of the diagonal (left), the cross peaks from (a) (middle) and the cross peaks from (b) (right) for comparison of sensitivity. The experiment time of the 2D experiment is less than two minutes.

STMAS experiment yields sharp ridges in the 2D spectrum as shown in Figure 1. A tilt of the 2D spectrum results in the isotropic chemical and quadrupolar shift along the indirect dimension that separates the MAS powder patterns of the second-order quadrupolar effect. Satellite transitions are NMR-allowed transitions and they also share energy levels with the observed central transition. Therefore the excitation and coherence transfer of the satellite transition coherence can be obtained efficiently using short rf pulses. The advantage of high spectral resolution and sensitivity along with the information available on quadrupolar coupling make the satellite transition MAS a very useful NMR experiment especially at high magnetic fields for the study of solid materials containing half-integer quadrupolar nuclei.

- ¹ Samoson, A., *et al.*, *Mol. Phys.*, **65**, 1013 (1988).
- ² Llor, A. and Virlet, J. *Chem. Phys. Lett.*, **152**, 248 (1988).
- ³ Frydman, L. and Harwood, J.S., *J. Am. Chem. Soc.*, **117**, 5367 (1995).

Complete Cross-Validation and R-Factor Calculation of Solid-State NMR Derived Structures

Kim, S., NHMFL/FSU, Molecular Biophysics
 Kovacs, F., NHMFL/FSU, Molecular Biophysics
 Quine, J., NHMFL/FSU, Mathematics and Molecular Biophysics
 Cross, T.A., NHMFL/FSU, Chemistry and Molecular Biophysics

We have developed a structural quality assessment method for a refinement procedure using solid-state NMR data. A validation method of solid-state NMR derived structure is required to choose the optimum weighting factor for the total penalty function that is achieved by balancing the contribution of the experimental constraints and the energy function. Complete cross-validation has been used to avoid the over-fitting of solid-state NMR derived structure using orientational constraints. The idea of cross-validation using the solid-state NMR data involves partitioning of experimental data into a test set and a working set and checking the free R-value during the refinement process. This approach is similar to the method used in crystallography and solution NMR. Optimizing the weighting factor on the penalty function by cross-validation will increase the quality of the refinement structure using solid-state NMR data.

Structural refinement using solid-state NMR data includes developing a model structure from orientational constraints derived from the anisotropic nuclear spin interactions. Orientational constraints are derived from the anisotropic nuclear spin interactions observed by solid-state NMR of uniformly aligned samples. The strategy for refining the structure involves setting up a penalty function that incorporates all available solid-state NMR data and the energy function. The constraints imposed on the gramicidin A structure during refinement are 19 ¹⁵N and 2 ¹³C anisotropic chemical shifts, 14 ¹⁵N-¹³C and ¹⁵N-¹H dipolar splittings, 12 C α -²H and 54 other quadrupolar splittings, 10 N-O and 10 H-O hydrogen-bond distances for a total of 141 constraints.

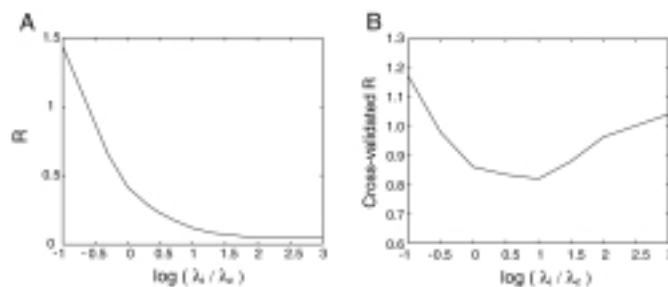


Figure 1. Influence of the weighting factor λ_i for total penalty on the refinement of the gramicidin A structure using solid-state NMR derived orientational constraints. $\lambda_e = 1$ kcal mol⁻¹ and the structural penalties are dimensionless units. (A) Weighted R value. (B) cross-validated weighted R value.

The free R-value decreased during the course of refinement, even though the test set has not been used in the refinement process. This indicates that the information content and the accuracy of the model increase during the refinement process. The expected R free value has less of a tendency for over fitting than R. The R free value can be used to prevent the user from over fitting the experimental data and increase the quality of refined structures.

Figure 1 shows the results from a series of calculations with 10 pairs of working and test data sets chosen at random and partitioned in a ratio of 90% to 10%. The λ_i s for the chemical shifts and dipolar splittings from the experiments were varied from 0.1 to 1000 kcal mol⁻¹. When the value of R-free reaches its minimum, the chemical shifts and the dipolar splittings in the test data sets are best predicted by refinement against those in the working data set. Thus, we can determine the optimal weighting factor λ_i .

- Brunger, A.T., *et al.*, *Science*, **261**, 328-331 (1993).
- Clore, G.M., *et al.*, *J. Am. Chem. Soc.*, **121**, 9008-9012 (1999).
- Ketchum, R.R., *et al.*, *Structure*, **5**, 1655-1669 (1997).
- Kovacs, F.A., *et al.*, *PNAS*, **96**, 7910-1915(1999).

Resolution Enhancement Using CPMG-HOMOGENIZED Detection of Solution NMR on the Keck Magnet

Lin, Y.-Y., Princeton Univ., Chemistry
 Ahn, S., Princeton Univ., Chemistry
 Garrett-Roe, S., Princeton Univ., Chemistry
 Warren, W. S., Princeton Univ., Chemistry
 Murali, N., NHMFL
 Brey, W., NHMFL
 Bowers, C.R., NHMFL/UF, Chemistry

Researchers interested in high-resolution NMR spectroscopy have long sought higher magnetic fields to enhance resolution and simplify spectra. Resistive or hybrid magnets can achieve substantially higher static fields than those available in

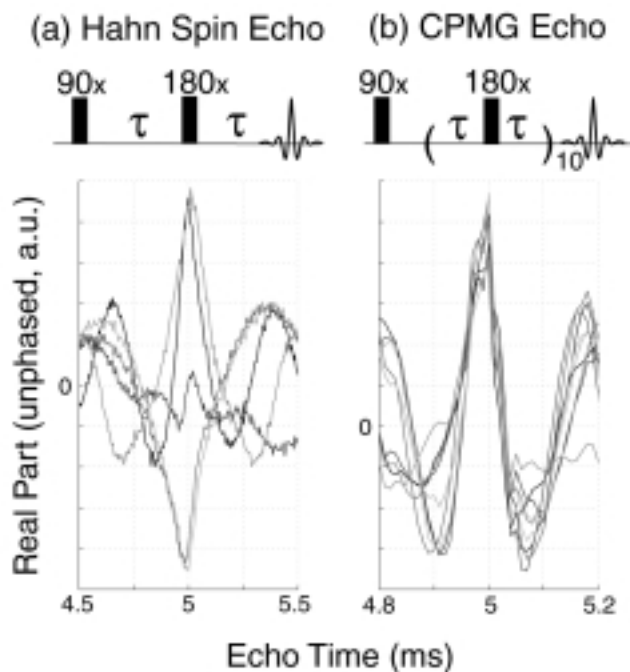


Figure 1. Spin echo generated by (a) Hahn echo sequence (5 superimposed), and (b) CPMG sequence (10 superimposed).

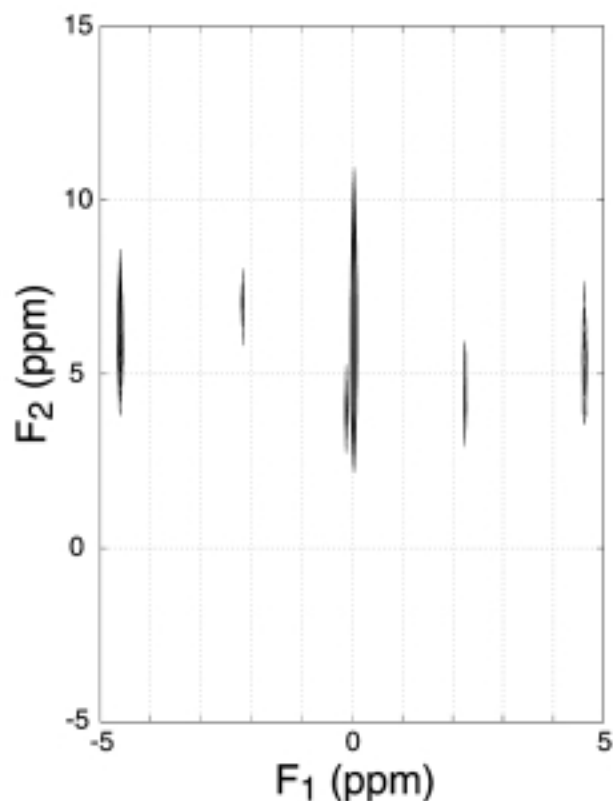


Figure 2. Experimental iZQC spectrum by CPMG-homogenized sequence.

superconducting magnets, but their *spatial uniformity* and *temporal stability* are unacceptable for high-resolution NMR applications.

A recently proposed detection method, termed “homogenized”, can remove spatial inhomogeneous broadening while retaining

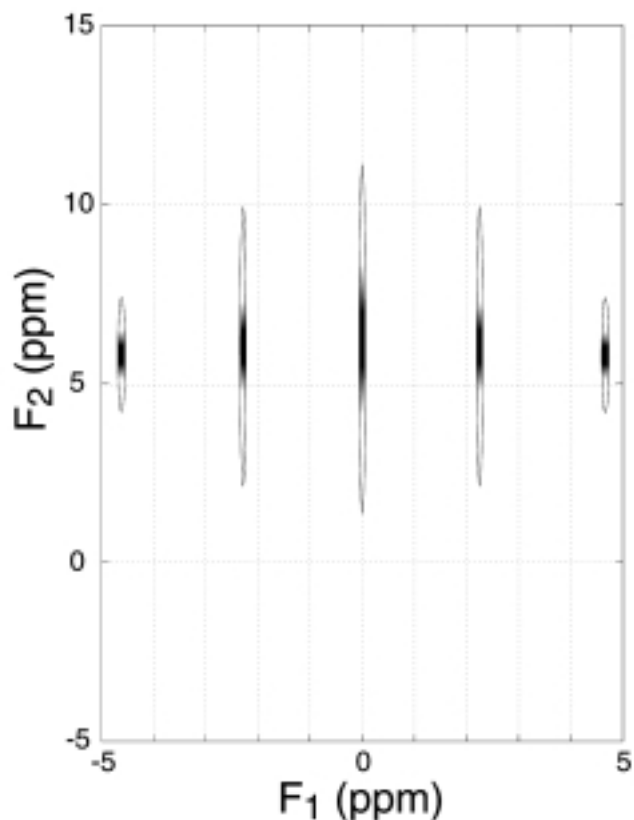


Figure 3. The corresponding simulated spectrum of Figure 2.

chemical shift differences and scalar couplings.¹ The homogenized sequence is based on observations of intermolecular zero-quantum coherences (iZQC) induced by the distant dipolar field between a solute molecule and solvent molecules that are micrometers away. The iZQCs evolve with no inhomogeneous broadening or drift effect, and are converted into solvent magnetization to be detected. For the Keck magnet, drift effects on the observed solvent magnetization must also be eliminated. This can be done with the Carr-Purcell-Meiboom-Gill (CPMG) pulse train shown in Figure 1. Pulse intervals $\ll 1$ ms give stable echoes in both phase and amplitude. Experimental effects of a CPMG-homogenized sequence on a 1:1 water/acetone sample are shown in Figure 2. The 1600 Hz linewidth is reduced in the indirectly-detected dimension to approximately 30 Hz, in accord with numerical simulations (Figure 3) based on modified Bloch equations.³ The iZQC spectrum shows the expected peak at the precise frequency difference with correct phase alternation, plus a peak at twice the difference (which is also expected with this sample).² Consequently, this demonstrates the *first ever high-resolution NMR spectrum* taken at very high magnetic field (>1 GHz).

Acknowledgements: This work was supported by NIH and NHMFL.

¹ Vathyam, S., *et al.*, *Science*, **272**, 92 (1996).

² Ahn, S., *et al.*, *J. Magn. Reson. A.*, **133**, 266 (1998).

³ Enss, T., *et al.*, *Chem. Phys. Lett.* **305**, 101 (1999).

⁴ Lin, Y.-Y., *et al.*, in preparation for *Phys. Rev. Lett.*

Analysis of Electrophoretic Transport Of Macromolecules Using Pulsed Field Gradient Nuclear Magnetic Resonance

Locke, B.R., FAMU-FSU College of Engineering,
Chemical Engineering

Moerland, T.S., FSU, Biology

Gibbs, S.J., NHMFL/FAMU-FSU CoE-CE

Acton, M., FAMU-FSU CoE-CE

The overall objective of the work performed on this project is to apply pulsed field gradient NMR spectroscopy (PFG-NMR) to the analysis of transport by diffusion, electrophoresis, and electroosmosis in porous media. The work performed during the last year has focussed on measurement of electroosmotic flow profiles by MRI in porous media consisting of solid, non-porous, spherical glass particles. Electroosmotic flow is the flow of water induced by an electrical field applied in a medium with fixed surface charges. Electroosmotic flow in porous media can have an important impact in many environmental or biological systems. MRI is an excellent tool to analyze flow in porous media, because it is not an invasive technique, and it does not require contrast agents or labels (at least for proton imaging). In the present study, solid glass spheres were placed inside a glass NMR tube containing a dilute salt solution. The sphere diameters were in two size classifications, ranging from 2.0 mm to 4.0 mm and 1.0 mm to 1.2 mm. Electrodes placed on either end of the NMR tube containing the spheres and buffer solution were used to generate flow. PFG-MRI was performed on the Bruker 600 MHz wide bore superconducting magnet.

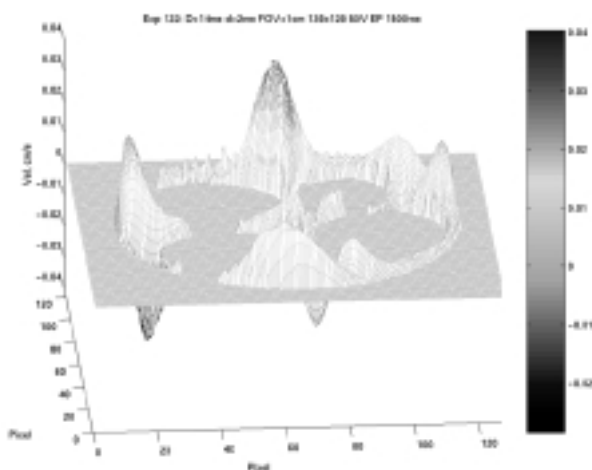


Figure 1. Transverse velocity map of electroosmotic flow in column containing 1 mm solid glass spheres. Flow reversal is evident by positive and negative peaks.

Images were taken at three locations near a single set of particles in order to capture a typical region containing pore space and solid material. Computational methods were used to generate velocity maps and to determine average velocities and dispersion coefficients at the various locations in the

sample. The inter-particle velocity profiles (Figure 1) showed patterns associated with flow reversal as has been shown for electroosmotic flow in a single closed tube without particles. These results provide quantitative information on the magnitudes and spatial resolution of flow induced by electrical fields in porous materials.

Acknowledgement: This project is supported by NASA through grant UGS95-0041.

Analysis of Transdermal Drug Delivery via Electroporation and Iontophoresis Using Pulsed Field Gradient NMR

Locke, B.R., FAMU-FSU College of Engineering,
Chemical Engineering

Moerland, T.S., FSU, Biology

Gibbs, S.J., NHMFL/FAMU-FSU CoE, CE

Caban, J., FSU, Institute of Molecular Biology

McFadden, L., FSU, Biology

Recent studies have shown that transdermal drug delivery can be enhanced by the application of electrical fields, alone and in combination with various chemical penetration enhancing compounds. A detailed understanding of the mechanism by which electrical fields and chemical penetration enhancing compounds affect transport in skin is not available however. Therefore, the present study was conducted, to use magnetic resonance methods to elucidate transport pathways and skin structure when electrical fields and chemical penetration enhancing compounds are applied to skin.

The focus of the work during the present year was to perform preliminary experiments on the effects of various types of penetration enhancing compounds on skin structure and water D_{app} . Analysis of diffusion maps of skin exposed to urea and obtained by MRI reveals that treatment has a statistically significant effect on water mobility: D_{app} in hair follicles was $3.5 \times 10^{-6} \text{ cm}^2 \text{ s}^{-1}$ and $4.2 \times 10^{-6} \text{ cm}^2 \text{ s}^{-1}$ in the absence and presence of urea, respectively. In the viable epidermis, administration of urea results in an increase of D_{app} from $2.6 \times 10^{-6} \text{ cm}^2 \text{ s}^{-1}$ to $3.8 \times 10^{-6} \text{ cm}^2 \text{ s}^{-1}$. In general, urea tends to highlight (i.e. enhance D_{app}) regions that contain more water, such as the viable epidermis and the hair follicles. This result suggests that the primary mode of action for this compound in facilitating transdermal transport is to enhance aqueous pathways. Work is



Figure 1. ^{19}F μMR image of skin from hairless rats. Darker regions highlight hair follicles and viable epidermis and light regions show dermis and stratum corneum.

proceeding to investigate combinations of electrical fields with chemical penetration enhancers. The specific goal is to identify the relative contributions of electroosmotic flow and diffusion in the various regions of the skin.

We are also investigating the mode of action of penetrant enhancers and the mobility of solutes by mapping the spatial distribution of ^{19}F containing penetrant enhancer and drug analogs within skin. ^{19}F μMR imaging as shown in Figure 1 is a promising technique for elucidating the transport pathways of a wider range of molecular solutes in the skin.

Magnetic Resonance Imaging of Non-Uniform Flow in Porous Media **IHRP**

Park, J., FAMU-FSU College of Engineering, Chemical Engineering/NHMFL

Pavlovskaya, G.E., FAMU-FSU CoE-ChE/NHMFL

Gibbs, S.J., FAMU-FSU CoE-ChE/NHMFL

Pulsed field gradient (PFG) MRI methods have been applied to study non-uniform flow in porous media. The specific focus has been upon improving flow distribution in packed chromatographic columns. Two basic model systems have been studied: a cylindrical sponge-like material with a hollow central core; and a chromatographic column packed with various beads. The former model is useful for understanding the role of transverse momentum transfer in porous media with transverse permeability variations. Figure 1 shows a comparison of the measured velocity profile in the cylindrical sponge-like sample and a fit of a model based upon Brinkman's description of flow in porous media. The theoretical description appears adequate and our observations confirm the interpretation that transverse momentum transfer is only significant for length scales on the order of the pore size. Measurements of flow non-uniformity in packed columns of beads show non-uniformities over much larger length scales than the pore size. Figure 2 shows such non-uniformities; these are thought to be due to both packing density variations and the effects of a non-ideal header or flow

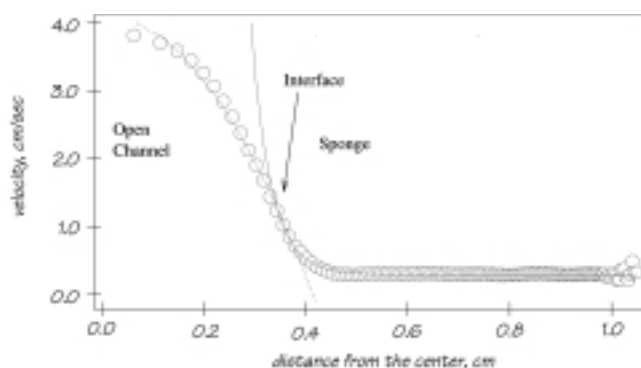


Figure 1. Comparison of theory and experiment for the radial profile of axial fluid velocity for flow in a porous medium with a transverse permeability discontinuity.

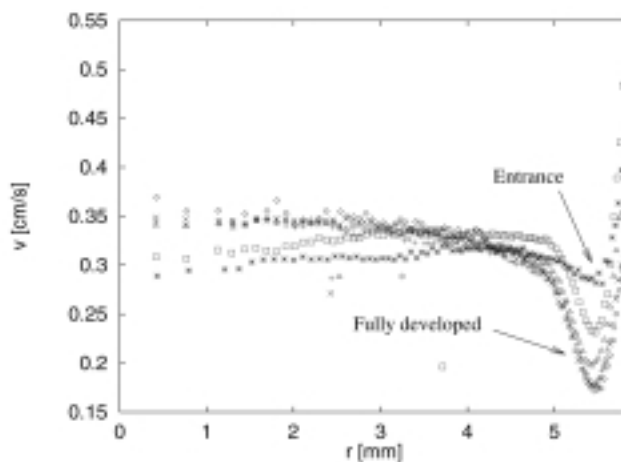


Figure 2. Flow development in a column packed with 99 μm polystyrene beads. Shown are radial profiles of axial velocity for different distances from the column entrance. The data show both that the packing density is radially nonuniform and that the distributor significantly effects the flow field.

distributor at the entrance of the column. Future work will focus on a systematic investigation of the relationship of bead properties, packing method and packing density variations and of improved header designs.

Rapid Computational Techniques for Estimating Velocity and Apparent Diffusion from PFG NMR Data

Raghavan, K., FAMU-FSU College of Engineering, Chemical Engineering/NHMFL

Gibbs, S.J., FAMU-FSU CoE-ChE/NHMFL

Computational methods to estimate velocities and diffusion coefficients from pulsed field gradient (PFG) NMR data have been implemented and compared for synthetic data and for experimental data from flow in porous media. For many situations, PFG NMR data take the form of a Gaussian damped sinusoid with the frequency representative of the flow velocity and the damping factor representative of the apparent diffusion coefficient. It is often desirable to sample the PFG data sparsely in the motion encoding wave vector in order to save acquisition time and non-uniformly in order to improve accuracy; these non-uniformly sampled data are not amenable to analysis by the FFT algorithm. We have investigated two objective functions applicable to non-uniformly sampled data: the Scargle Periodogram (SP) and a Bayesian probability function based upon the Gaussian model. These objective functions have been optimized by either simulated annealing or a genetic algorithm. Both approaches are robust to the presence of noise, but the simulated annealing method is faster. The SP approach involves a one dimensional search and is hence fast, but does not permit error estimates. Methods have been compared with the Levenberg-Marquardt method for the same data. The method of choice has been found to be the simulated annealing of the Bayesian probability function; estimates of velocity and

apparent diffusion coefficients (and associated confidence intervals) can typically be performed in a few milliseconds on a 200 MHz Pentium processor for on the order of ten samples of the motion encoding wave vector.

High-Field Resolution Enhancement in ^1H MAS NMR

Samoson, A., National Institute of Chemical Physics and Biophysics, Tallinn, Estonia
Gan, Z., NHMFL

High resolution ^1H NMR spectroscopy in solids has been a challenge for over 30 years. Pioneering work of Waugh, Huber and Haeberlen¹ demonstrated a multipulse linewidth narrowing approach in 1968, and this has remained the principal approach to resolution enhanced measurements. Combined with slow magic angle spinning, susceptibility limited linewidth can in principle be achieved. Despite considerable attention to the method, however, only relatively few applications to structural problems have been published. This can be explained by experimental difficulties in tuning pulse sequences and very stringent power handling capabilities posed to both amplifier and probe. Special attention also has to be given to spectral scaling factor and preparation of the sample. Experimental difficulties are complicated at higher fields, as broader spectral span requires more pulse power, whereas power amplifiers actually become less efficient.

A straightforward magic angle spinning technique has not been efficient in suppressing homonuclear dipolar interactions, as residual linewidth reduces only linearly with spinning frequency. In the case of tightly coupled hydrogen nuclei residual line width still exceeds useful chemical shift range under experimental conditions available until very recently.

Advances in both magnet and spinning technology now begin to change the situation. Lines separate linearly with the magnetic field, whereas homonuclear dipolar linewidth remains constant or even reduces slightly due to quenching of spin flip-flop terms. This means reduction of relative linewidth in ppm scale. Absolute reduction of linewidth is achieved with spinning, approaching the value of static line broadening. Both effects lead to a virtually quadratic improvement in resolution. We demonstrate first high resolution spectra of a tightly coupled hydrogen spin system, registered without multipulse manipulation in spin space.

The highest MAS speed reached by rotor is determined by balance of centripetal force and tensile strength of the rotor wall material. The force can be reduced by decreasing the diameter of the rotor. A special probe, constructed at the National Institute of Chemical Physics and Biophysics, Estonian Academy of Sciences, with partially stabilized zirconia rotors of less than 2 mm diameter enables sustained speeds over 40 kHz.

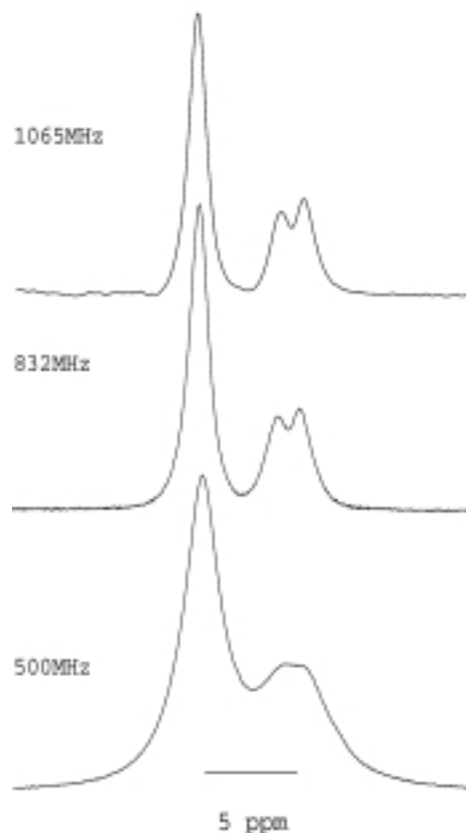


Figure 1. ^1H MAS (40 kHz) spectra of glycine at 11.7, 19.5, and 25 T.

Test measurements were carried out at 832 and 1065 MHz resonance frequency, provided by superconducting and resistive Bitter type magnets respectively. The magnets are the strongest of their kind currently available. Spectra of glycine, spun at 40 kHz, are shown in the figure. A spectrum acquired at medium field with resonance frequency 500 MHz is presented for comparison. A significant resolution improvement with field intensity is evident. Apart from providing means for reliable and fast high resolution hydrogen spectroscopy, high-field-fast-spinning approach also opens new possibilities for more sophisticated multidimensional and multinuclear correlation NMR.

¹ Waugh, J.S., *et al.*, Phys. Rev. Lett., **20**, 180 (1968).

FT-ICR Mass Spectrometry in a High Homogeneity 25 T Resistive Magnet

Shi, S.D.-H., NHMFL/FSU, Chemistry
Drader, J.J., NHMFL
Hendrickson, C.L., NHMFL
Marshall, A.G., NHMFL/FSU, Chemistry

Many performance parameters of FT-ICR mass spectrometry improve dramatically with increasing magnetic field. Our prior results from a 20 T resistive magnet showed that performance

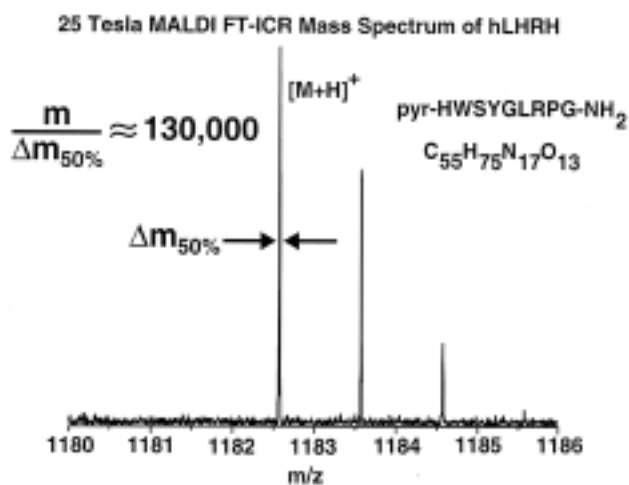


Figure 1. 25 T MALDI FT-ICR mass spectrum of hLHRH.

was limited by the large spatial inhomogeneity in spite of the high field. In this paper, we compare MALDI mass spectra at the same magnetic field for two resistive magnets with different field spatial homogeneity. In addition, we report MALDI spectra at 25 T—the highest magnetic field for FT-ICR to date (see figure). The first broadband FT-ICR mass spectrum (poly(ethylene glycol) 2000) from a resistive magnet is accurately fitted by the standard ICR mass calibration function.

Acknowledgements: The authors thank John P. Quinn and Daniel G. McIntosh for help in building this instrument. This work was supported by grants from NSF (CHE-94-13008), The W. M. Keck Foundation (Los Angeles, CA), Florida State University, and the NHMFL in Tallahassee, FL.

¹ Shi, S.D.-H., *et al.*, *J. Am. Soc. Mass Spectrom.*, **10**, 265-268 (1999).

NMR Detection of Bitter Magnet Temporal Fluctuations

Sigmund, E., Northwestern Univ. and Science and Technology Center for Superconductivity

Mitrovic, E., NWU, STCS

Bachman, H., NWU, STCS

Thomas, G., NWU, STCS

Calder, E., NWU, STCS

Halperin, W., NWU, STCS

Kuhns, P., NHMFL

Reyes, A., NHMFL

Moulton, W.G., NHMFL

We have used NMR spin-spin relaxation measurements to probe the temporal instability of the Bitter magnets at the NHMFL. An NMR relaxation measurement repeated many times in an unstable applied field will show a phase dispersion due to that

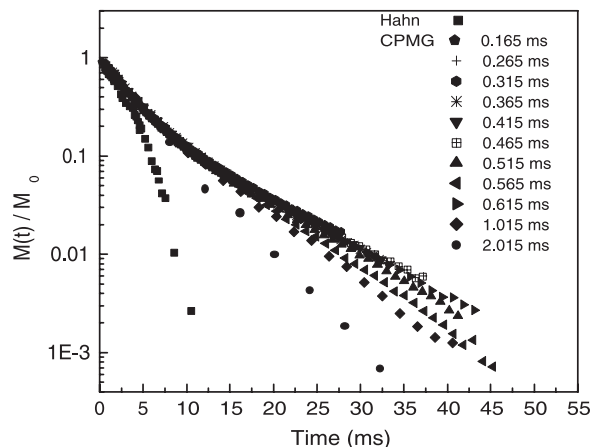


Figure 1. DGS spin-spin relaxation at 23 T.

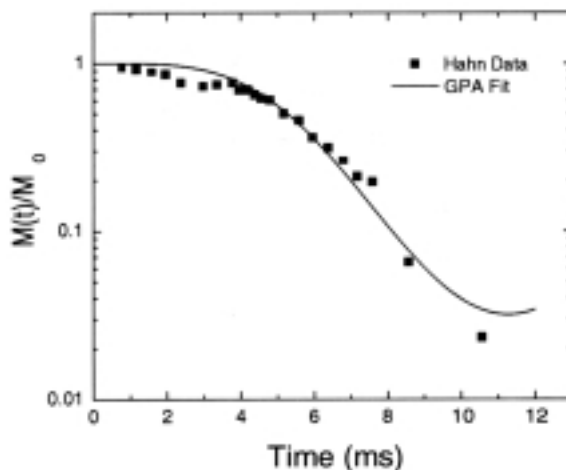


Figure 2. Hahn-echo residual decay fit from the 23 T data of Figure 1.

instability. Choosing a sample whose intrinsic dephasing is easily separated thus allows a study of the spectral distribution of the applied field. Our sample was deuterated glycerol in a silica gel (DGSG), chosen so as to minimize diffusive dephasing in the background magnetic field gradient.

The results of 2D spin-spin relaxation measurements in the 23 T, Cell 7 Bitter magnet are shown in Figure 1. Two sequences were performed: Hahn echo and Carr-Purcell-Meiboom-Gill (CPMG) multiple echo. Since many rapid inversions of the magnetization tend to preserve its coherence from sweep to sweep, the CPMG decays with small interpulse delays are unaffected by the magnet's instability and dominated by the material's intrinsic dephasing. But as the inversions are more and more delayed until only one is applied per excitation (the Hahn echo sequence), the measured signal decay becomes more pronounced.

Removing the intrinsic part of the Hahn profile (as determined from CPMG sequences) we fit the residual decay to extract information on the field fluctuations in Figure 2. We use a single-harmonic field variation and a random phase approximation for the phase dispersion it generates. This model has been tested on spin-spin relaxation measurements with single-harmonic field

variations, and it extracts the applied fluctuations to within 10%. The fit of the 23 T Bitter magnet Hahn decay shows instability in the range $30 < \nu < 130$ Hz at a level of 0.4 ± 0.1 ppm, consistent with direct measurements of the power supply fluctuation spectrum. Having conclusively identified this source of systematic decoherence, we are developing means to eliminate it. One solution is to average in the polar rather than Cartesian domain; this approach works well but is limited to strong signals. An alternate hardware solution we are also pursuing is the use of a helium-cooled copper Faraday shield.

Acknowledgements: This work is supported in part by the NSF (DMR 91-20000) through the STCS.

GAMMA Calculations in Large Stray Field Gradients

Smith, S.A., NHMFL

Kinchesh, P., Queen Mary and Westfield College, Univ. of London

Randall, E.W., Queen Mary and Westfield College, Univ. of London

Calculations using the GAMMA¹ magnetic resonance simulation platform provide detailed insight into the nature of experiments performed in the presence of large stray field (STRAFI) gradients.² We have refined and considerably extended the previous initial use of GAMMA in calculating STRAFI NMR responses in a 50 T/m gradient³, a value that is typically encountered in the stray fields of superconducting magnets.

Previous studies of STRAFI echoes include the treatments of Benson and McDonald, which utilized the delta approximation in a Bloch treatment^{4,5} and of Bain and Randall, which used a density operator approach⁶. GAMMA employs a density operator approach, can readily eschew the delta approximation, and takes into account the change in the tip angle and the phase of the signal across the selected slice. It is the first treatment that can include relaxation in the calculation of echo intensities that are produced by RF pulse trains.

Some of the areas that have been (and are) under investigation:

1. Slice selection in large gradients: the effects of pulse shape, pulse duration, sample line-width, and spin locking
2. The variation in intensity of echoes as a function of pulse power and duration for rectangular, Gaussian, sinc, and other shaped pulses
3. The use of "ideal" pulses and the validity of the delta approximation
4. The effects of relaxation on echo intensities produced by the application of RF pulse trains
5. Possible use of phase cycling in STRAFI pulse sequences.

GAMMA is currently the best tool available for STRAFI simulations, and we anticipate it will be in frequent use in this capacity as the NHMFL pursues its planned involvement in STRAFI experiments.

- 1 Smith, S.A., *et al.*, J. Magn. Reson. Ser. A, **106**, 75 (1994).
- 2 McDonald, P.J. and Newling, B., Reports on Progress in Physics, **61**, 1441 (1998).
- 3 Randall, E.W. and Smith, S.A., Joint 29th Ampere – 13th ISMAR International Conference, Berlin, 1, 571 (1998).
- 4 Benson, T.B. and McDonald, P.J., J. Magn. Reson., **109B**, 314 (1995).
- 5 Benson, T.B. and McDonald, P.J., J. Magn. Reson., **112A**, 17 (1995).
- 6 Bain, A.D. and Randall, E.W., J. Magn. Reson., **123A**, 49 (1996).

GAMMA: The Magnetic Resonance Simulation Package

Smith, S.A., NHMFL

The NHMFL has continued its support of the premier package for magnetic resonance simulations, GAMMA. GAMMA is a C++ library expressly for simulation of magnetic resonance experiments and written by Scott A. Smith¹. It is used in hundreds of institutions worldwide and its calculations play a part in numerous publications each year. Herein is a brief report of important work done at the core level of GAMMA and alterations to the much used WWW site that provides the package to those outside the NHMFL.

At the inception of GAMMA, a somewhat risky choice was made to build the platform using the relatively new



Figure 1. The entry point of the new GAMMA WWW site, <http://gamma2.magnet.fsu.edu/>

C++ computer language. Fortunately in the last decade C++ became the dominant programming language for demanding applications. It is now the choice of professional programmers for sophisticated applications and is used by more than 1.5 million programmers worldwide. It was not until September 1998, however, that the ISO/ANSI C++ approved standard was published. Virtually all C++ compilers have since attempted to become ANSI compliant and subsequent GAMMA compatibility issues arose. The GAMMA source codes, available to the public with the package, have been fully updated to ANSI standards this past year. This allows users to build GAMMA from sources using any ANSIC++ compiler, and such compilers are now running on all computers, from the most powerful supercomputers down to the ubiquitous personal computer. Ports of the GNU C++ compiler are freely obtainable, as is GAMMA, and hence users of the platform remain unhindered from excessive software costs.

In order to keep pace with internet advancements the GAMMA WWW site has been extensively revised (Figure 1). The bulk of the site was rewritten to utilize the GNU M4 macro processor, accommodating rapid content rebuilding for both local documentation and GAMMA mirror sites. Users may now download personal copies of web-based documentation that is viewable using any modern WWW browser. Akin to the site itself, local documentation contains numerous tutorials and examples, instructions for downloading and installation, as well as manuals in both PDF and HTML formats that explicitly define GAMMA classes and functions. The local documentation ties in seamlessly with the WWW site using hypertext links. In anticipation of additional GAMMA mirror sites, the mentioned changes provide the means to generate such sites specifically tailored for system and location needs.

¹ Smith, S.A., *et al.*, J. Magn. Reson. Ser. A, **106**, 75 (1994).

Transient EPR at 240 GHz in Ruby

Van Tol, J., NHMFL
Brunel, L.-C., NHMFL

In order to measure EPR in short-lived intermediates and excited states, we have constructed a heterodyne EPR spectrometer operating at 120, 240, and 360 GHz. The high millimeter-wave frequencies have the important advantage of decreasing the timescale of the experiment with respect to conventional EPR frequencies around 10 to 35 GHz, and one of our principle goals is to study for the first time paramagnetic systems with sub-nanosecond lifetimes.

For optimum sensitivity we have designed a heterodyne quasi-optical spectrometer with Schottky-diode detection, which at room temperature was measured to have a CW-sensitivity of 10^{-11} spins/Gauss without a cavity, and 10^{-9} spins/Gauss with a Fabry-Perot type cavity. Optical excitation of these short-lived paramagnetic systems is achieved with laser-pulses from

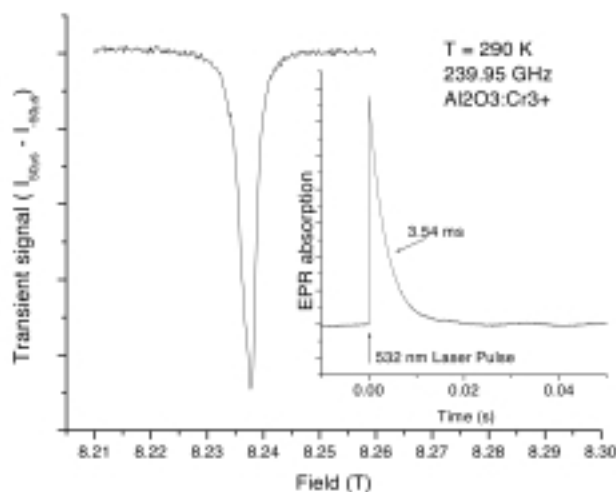


Figure 1. Transient EPR-signal at 239.95 GHz. Signal corresponds to depletion of the $m_s = -3/2$ to $m_s = -1/2$ transition in the $4A_2$ ground state of Cr^{3+} in Al_2O_3 . The inset shows the mono-exponential decay of the signals at 8.25 T.

either a 5ns Q-switched Nd:YAG laser or a 120 ps mode-locked Nd-YAG with an OPG.

The first transient signals at 240 GHz were observed at room temperature in ruby ($Al_2O_3:Cr^{3+}$). The $4A_2$ ground state gives rise to an EPR spectrum with three distinct transitions, whereas the optical excitation populates a $2E$ meta-stable excited state with a lifetime of around 3 ms. We thus should be able to measure both the transient EPR in the excited state, as well as the depletion of the ground state. At room temperature, however, only the latter was observed (see Figure 1). The transient signals show a 3.5 ms mono-exponential decay from the excited state. The main extensions to the current experimental setup will be a Fabry-Perot cavity operating at low temperatures, an extension of the spectrometer to super-heterodyne detection, and the introduction of a sample-flow system.

Phase Correction for Collision Model Analysis and Enhanced Resolving Power of Fourier Transform Ion Cyclotron Resonance Mass Spectra

Vining, B.A., FSU, Chemistry
Bossio, R.E., FSU, Chemistry
Marshall, A.G., NHMFL/FSU, Chemistry

Phase correction of FT-ICR data yields an absorption spectrum that offers a gain by up to a factor of 2 in mass resolving power (at half-maximum peak height), compared to conventional magnitude-mode display. That improvement is equivalent to doubling the applied magnetic field strength, without loss in signal-to-noise (S/N) ratio, provided that the time-domain data is padded with an equal number of zeroes before FFT. Our simple, visual, user-interactive algorithm quickly corrects for zero-order and first-order variation of phase with frequency. We find that the theoretical mass resolving power enhancement for

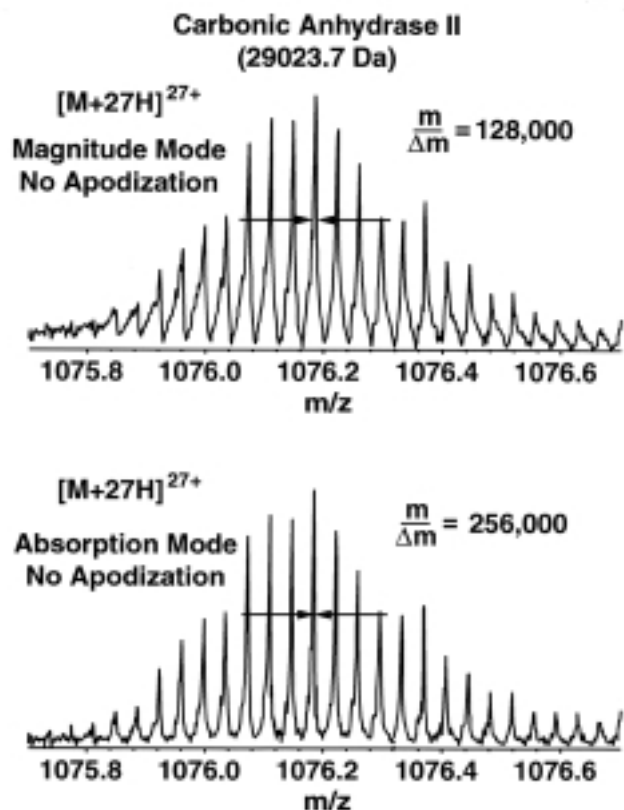


Figure 1. FT-ICR spectra before and after phase correction.

pressure-limited absorption-mode over magnitude-mode line shape depends on the collision mechanism: factor of 1.40 for hard-sphere vs. $\sqrt{3}$ for Langevin (ion-induced dipole). Thus, the experimental enhancement in mass resolving power (factor of 1.43 ± 0.09) for isotopically resolved peaks in the FT-ICR mass spectra of electrosprayed bovine carbonic anhydrase (~29 kDa) directly supports the hard-sphere collision model (see figure). Phased FT-ICR spectra should prove especially desirable for analysis of complex mixtures, for resolving isotopic distributions in electrosprayed multiply-charged macromolecules, and for characterizing ion collisions (and thus ion size and shape).

Acknowledgements: We thank Stone D.-H. Shi for frequent and helpful assistance with the MIDAS analysis code, and J. J. Drader for help in acquiring signals with the MIDAS data station. We also thank Christopher L. Hendrickson and Forest M. White for helpful conversations and insights. This work was supported by the NSF National High Field FT-ICR Facility (CHE-94-13008), NIH (GM-31683), Florida State University, and the NHMFL at Tallahassee, Florida.

¹ Vining, B., A. *et al.*, *Anal. Chem.*, **71**, 460-467 (1999).

Creation of Octupole Nuclear Spin Polarization by Optical Pumping in Strained GaAs/AlGaAs Quantum Wells

Vitkalov, S.A., UF, Chemistry

Bowers, C.R., UF, Chemistry

Simmons, J.A., Sandia National Laboratories

Reno, J.L., Sandia National Laboratories

Here, an optically pumped NMR study on an AlGaAs/GaAs multiple quantum well (MQW) film is reported. The wavelength dependence of the optically pumped NMR enhancement was recorded, and the experiments resulted in a determination of the hyperfine coupling of the MQW nuclear spins with the 2DES. Also, a quenching of nuclear spin diffusion due to strain in MQW layers was observed and analytically modelled.

The sample consisted of a high mobility MQW film consisting of 21 GaAs wells with Si doped $\text{Al}_{0.1}\text{Ga}_{0.9}\text{As}$ barriers, grown by molecular beam epitaxy (MBE) on a GaAs substrate. To eliminate the background GaAs NMR signal due to the substrate, it was removed by chemical etching, and the thin QW film was fixed with epoxy to a silicon support. The NMR spectra were recorded at 3 T. This magnetic field was chosen to obtain the $\nu=1$ filling factor. The optically pumped ^{71}Ga NMR spectra obtained at two different laser wavelengths are shown in Figure 1. No Knight shift was observed at 4.2 K, presumably due to the relatively high temperature and low electron density of this sample. A small Knight shifted component (<5 kHz) could be resolved at lower temperature, but not well enough to permit a filling factor dependence study by rotation of the sample.

The ^{71}Ga spectra consisted of 3 lines separated by 55 kHz, each having a line width of 3 KHz. The 55 kHz quadrupole splitting results from the planar stress caused by the difference in the thermal expansion coefficients of the GaAs film and the Si support. Remarkably, the satellite transitions always exhibited an antiphase relationship with respect to the central transition. With longer optical pumping irradiation times, the central peak is seen to grow disproportionately, saturating on a substantially longer time-scale compared to the growth of the satellite transitions. Evidently the polarization of the satellite transitions cannot spin diffuse into the barriers due to the mismatch in transition energy with the AlGaAs satellites which experience a substantial first order quadrupole broadening due to the presence of 10% aluminum.

The optical pumping enhancement was found to vary dramatically with wavelength. The spectra undergo several striking 180° phase inversions. For instance, at 812.9 nm a total phase inversion results when the laser wavelength is increased by only 0.335 nm (150 GHz). The phase inversions are attributed to spin state selective optical pumping. The antiphase NMR line shape is consistent with the existence of an unusual octupole polarization with an admixture of dipole polarization.

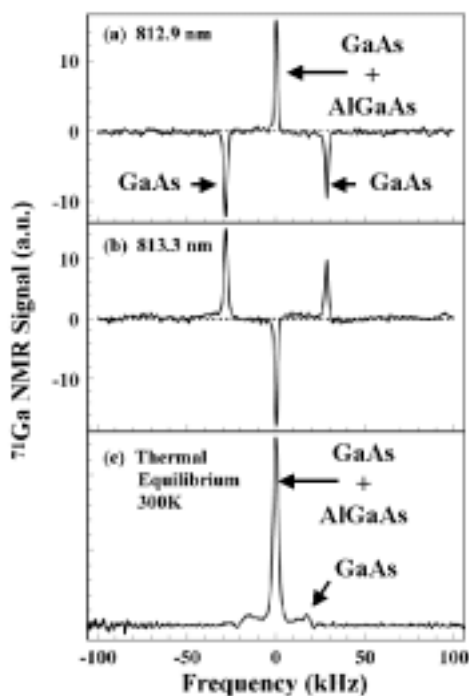


Figure 1. Optically pumped gallium-71 FT-NMR spectra obtained at 4.2 K. (a) and (b) were obtained with optical pumping laser wavelengths differing by only 0.4 nm. (c) The 300 K spectrum of the same sample after averaging 30,000 transients.

The detailed electron-nuclear cross-relaxation mechanism that creates this previously unobserved nuclear spin order remains to be elucidated.

From the measured enhancement factor, defined as the ratio of the signals obtained under optical pumping conditions and at thermal equilibrium, it is possible to estimate the nuclear spin polarization. Independent measurement of the nuclear spin polarization and Overhauser shift (the change in ESR resonance frequency in proportion to the nuclear spin polarization) allowed the first experimental determination of the hyperfine coupling constant between the QW nuclei and the extended electronic states of the 2DES at $\nu=1$. An enhancement factor of 8.4, obtained for the central transition following a 40 s optical excitation at 801.5 nm, corresponded to an estimated polarization of 3.2×10^{-3} .

Development of Orientational Constraints from ^{19}F Labeled Peptides

Wang, J., NHMFL/FSU, Institute of Molecular Biophysics
 Grage, S., Univ. of Jena, Germany, Institute of Molecular Biology
 Ulrich, A., Univ. of Jena, Germany, Institute of Molecular Biology
 Fu, R., NHMFL
 Cross, T.A., NHMFL/FSU, Chemistry

^{19}F NMR has proven to be a powerful technique in the study of protein structure and dynamics because the ^{19}F nucleus is

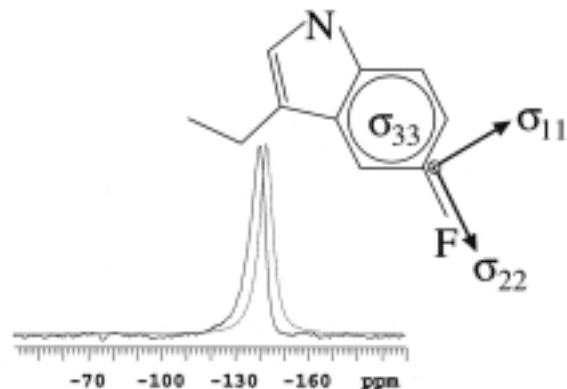


Figure 1. Assignment of 5- ^{19}F -CSA tensor axes in 5F-Trp. Based on known Trp side chain orientation, the expected oriented spectra for the six basic tensor assignments were simulated and compared with the experimental spectrum. Here, only the best fit is shown.

easily incorporated at specific labeling sites, where it provides a relatively non-perturbing yet sensitive probe with no background signals.¹ Here, the ^{19}F chemical shift anisotropy (CSA) tensor in the molecular frame of the labeled tryptophan was evaluated in the light of the gramicidin A (gA) peptide structure derived from solid-state NMR.² ^{19}F orientational constraints can be incorporated into the structural and dynamics study of tryptophan in gA, which has been known to play a significant role in the function of this channel.

Based on the known 5F-Trp side chain coordinates for Trp-13 in gA in oriented lipid bilayers, which has been determined by ^2H NMR,³ we have characterized the ^{19}F -CSA tensor orientation for this site. Assuming a perfect alignment of the tensor axes along the C-F bond, the indole ring normal, and a third in-plane axis, there are six possibilities for assigning the tensor axes. Of these, two are in good agreement with our ^{19}F -NMR measurements on samples aligned with the bilayer

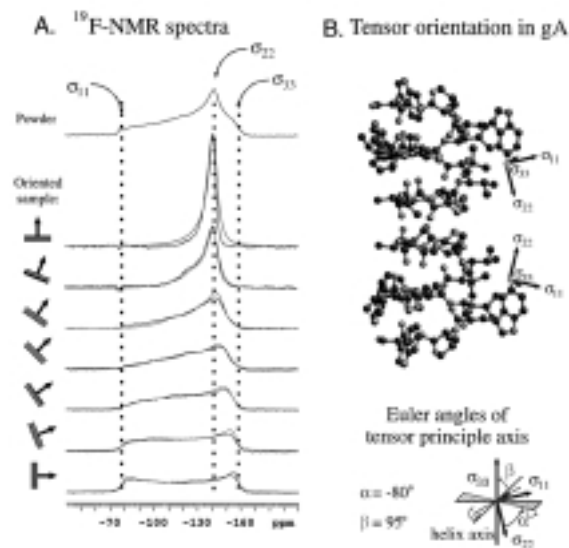


Figure 2. 4F-Trp tensor orientation determination by spectra simulation of oriented gA sample with various tilt angles.

normal parallel to the magnetic field (Figure 1). Tilting the oriented sample allows a more detailed characterization of the tensor orientation. The best fit was found with σ_{22} aligned along the CF bond, σ_{33} perpendicular to the tryptophan plane, and σ_{11} in-plane (the Euler angles relating the principal axes to the sample normal are $\alpha=-84^\circ$, $\beta=114^\circ$). Without restricting the tensor elements to the molecular symmetry axis frame, an improved fit is possible, where the tensor is slightly tilted away from the symmetry axes. (Euler angles: $\alpha=-80^\circ$ and $\beta=95^\circ$). The best fit of the simulated line-shapes to the tilt spectra series and the tensor orientations of 5F-Trp13 in gA are shown in Figure 2.

- ¹ Grage, L., *et al.*, *J. Magn. Reson.*, **138**, 98-106 (1999).
² Ketchum, R., *et al.*, *Science*, **261**, 1457-1460 (1993).
³ Cotten, M., *et al.*, Ph.D. Thesis, Tallahassee (1998).

Imaging Membrane Protein Helical Wheels

Wang, J., FSU, Institute of Molecular Biophysics (IMB)
 Denny, J., FSU, Mathematics
 Tian, C., FSU, IMB
 Kim, S., FSU, IMB
 Mo, Y., FSU, Chemistry
 Kovacs, F., FSU, IMB
 Song, Z., NHMFL
 Nishimura, K., NHMFL
 Gan, Z., NHMFL
 Fu, R., NHMFL
 Quine, J.R., FSU, Mathematics
 Cross, T.A., NHMFL/FSU, Chemistry

Solid-state NMR derived orientational constraints from samples with one, two or three dimensional order can be used to solve high resolution structure from a lamellar phase lipid

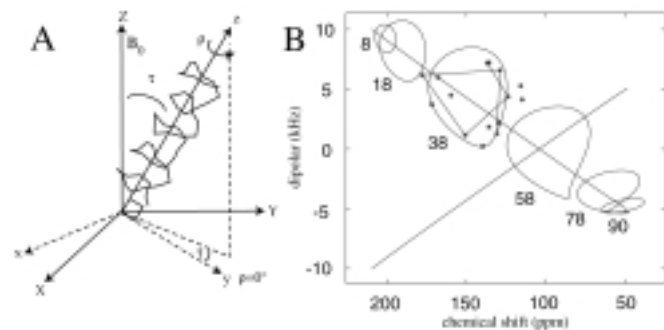


Figure 1. Origins of the PISA wheels. (A) Definitions of τ and ρ for an α -helix. (B) PISEMA experimental data (*) from selectively labeled transmembrane peptide of M2 Protein obtained at the 400 MHz. The helix tilt is determined to be $38 \pm 3^\circ$. A PISA wheel resembling a helical wheel is illustrated by connecting the resonances from several consecutive ^{15}N sites in the sequence resulting in the determination of the rotational orientation for this helix in a lipid bilayer.

environment. PISEMA (Polarization Inversion Spin Exchange at the Magic Angle) is a major improvement over previous experiments that correlate anisotropic dipolar and chemical shift interactions.¹ Recently we recognize that α -helices give rise to unique resonance patterns in PISEMA spectra, as summarized in Figure 1. The center of this pattern uniquely defines the helical tilt without a need for resonance assignments. The distribution of resonances from amino acid specific labels around the PISA wheel defines the rotational orientation of the helix and yields preliminary site specific assignments. With assignments high resolution structural details, such as differences in tilt and rotational orientation along the helical axis leading to an assessment of helical coiling can be obtained.

In a parallel and complementary study, Marassi and Opella have independently observed the same phenomena in the PISEMA spectra of membrane polypeptides.

- ¹ Wu, C.H., *et al.*, *J. Magn. Reson.*, **109A**, 270 (1994).

Structural Determination of the M2 Transmembrane Peptide (TMP) H⁺ Channel from Influenza A Virus

Wang, J., NHMFL/FSU, Institute of Molecular Biophysics
 Kovacs, F., NHMFL/FSU, IMB
 Kim, S., NHMFL/FSU, IMB
 Mo, Y., NHMFL/FSU, Chemistry
 Song, Z., NHMFL
 Cross, T.A., NHMFL/FSU, Chemistry

M2 is a 97 amino acid homo-tetrametric membrane protein located in the envelope of the Influenza A virus. It is generally believed that M2 functions as an H⁺ channel and participates in the virus uncoating process after viral uptake by endocytosis. This protein is also the target of an anti-viral drug amantadine. In the native protein the transmembrane domain of M2 corresponds to amino acids 26-43 and has been shown to be alpha-helical by circular dichroism spectroscopy. A synthetic 25-residue M2-TMP encompassing the transmembrane domain has been shown to form amantadine-sensitive ion channels in lipid bilayers, implying that transmembrane domain is responsible for the functional properties of the protein.¹ The aim of this work is to determine the M2-TMP structure with orientational constraints derived from solid-state NMR experiments.^{2,3}

The data shown in Figure 1 is from PISEMA spectra of multiple and single-site labeled preparations of M2-TMP in hydrated lipid bilayers in which the bilayer normal is aligned parallel to the magnetic field direction. The characteristic wheel pattern can be used to assess the coiling of alpha helices. With resonance assignments, minor changes in ρ and τ along the length of M2-TMP indicate a virtually straight alpha-helical structure.⁴

Moreover, in PISEMA spectra, the ^{15}N chemical shifts and ^{15}N - ^1H dipolar couplings of individual ^{15}N labels provide the orientational constraints to determine the orientation of specific

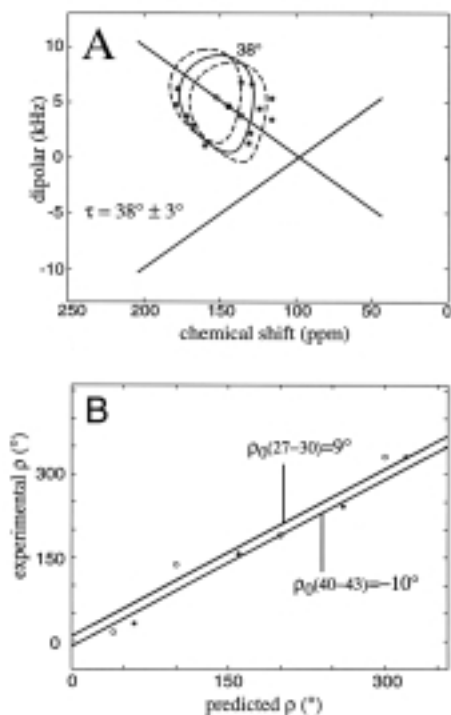


Figure 1. Segmental tau and rho determinations for the helical wheel pattern of PISEMA spectra of M2-TMP. Tau and rho values provide a unique way to characterize the orientation of M2-TMP.

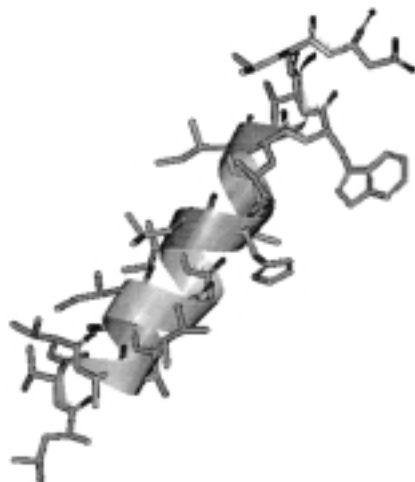


Figure 2. Refined M2-TMP monomer structure based on orientational constraints from solid state NMR.

peptide planes. Orientational ambiguities, which are inherent to the solid state NMR approach, can be addressed by calculating the local ρ and local τ value of each peptide plane. A unique orientation can be determined based on the fact that M2-TMP forms a right-handed alpha-helical structure. Once the unique orientations of a pair of adjacent planes (a diplane unit) are determined with respect to magnetic field, advantage of the tetrahedral geometry about the shared $C\alpha$ can be taken to define the relative orientation of the planes in terms of ϕ and ψ torsion angles. The initial M2-TMP structure has been built within Biosym based on the obtained torsion angles. The structure was then refined using the program TORC, which was developed in this group. The final M2-TMP monomer structure is presented in Figure 2.³

- ¹ Salom, D., *et al.*, *Biophys. J.*, **76**, A123 (1999).
- ² Kovacs, F.A., *et al.*, *J. Mol. Biol.*, in press (1999).
- ³ Wang, J., *et al.*, in preparation (2000).
- ⁴ Wang, J., *et al.*, *J. Magn. Reson.*, in press (1999).

Method for Removal of Magnetic Susceptibility Distortions in High-Field T_2^* -Weighted MR Imaging

Yang, Q.X., Penn St. Univ., Radiology
 Smith, M.B., Penn St. Univ., Radiology/Cellular and Molecular Physiology
 Briggs, R.W., UF, Radiology/Chemistry/Biochemistry and Molecular Biology
 Rycyna, R.E., Bruker Instruments

Development of high magnetic field MRI techniques for microimaging and in vivo imaging is hampered by the significant artifacts produced by B_0 inhomogeneities due to adjacent regions of differing magnetic susceptibility. Gradient Echo Slice Excitation Profile Imaging (GESEPI) has recently been introduced as a means of recovering signal lost to intravoxel phase dispersion originating from macroscopic local gradients in T_2^* -weighted MR images, and demonstrated to work effectively at field strengths up to 9.4 T.¹ Our experiments at the NHMFL were designed to test the usefulness of the method for correcting susceptibility artifacts at the highest field currently available for MR imaging.

Methods. Mouse brain gradient-recalled echo (GRE) images in the coronal plane were acquired at 14 T on a Bruker 600 WB Avance at the NHMFL with TR = 100 ms, 1 mm slice thickness, 128 x 128 matrix, and 20 mm FOV. GESEPI images were acquired with 32 G_C steps per image set with $G_C^{\max} = \pm 250\%$. Other images were acquired using similar parameters.

Results and Discussion. Figure 1 shows GRE and GESEPI images obtained of a phantom in a plane near an air-filled spherical capillary. Figure 2 shows 14 T images of a live mouse brain.

In summary, GESEPI has been shown to effectively remove susceptibility-based intravoxel dephasing artifacts and signal

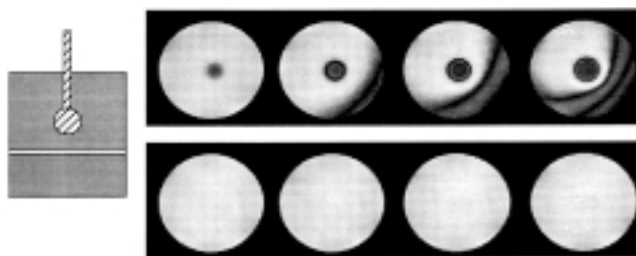


Figure 1. GRE (top) and GESEPI (bottom) phantom images in a plane near an air-filled sphere (insert, left). TE = 4, 10, 15, and 20 ms (left to right). $B_0 = 14$ T.

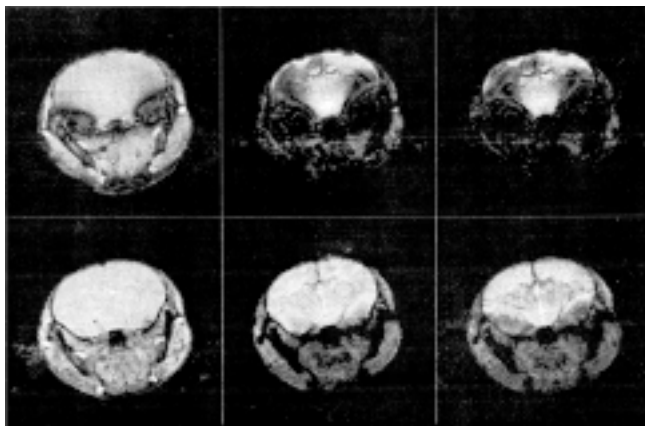


Figure 2. Live mouse brain GRE (top) and GESEPI (bottom) images. TE = 6, 15, and 20 ms (left to right).

loss in GRE images and to dramatically improve the quality of T_2^* -weighted images even at long TE times and at high field strengths. This method should be useful for obtaining T_2^* contrast from microscopic intravoxel field variations without the deleterious influence of artifacts from local macroscopic field gradients resulting from susceptibility differences within the sample. It is also important for use in fast multi-slice imaging in high-field whole-body MRI, where conventional fast-spin echo (FSE) methods of obtaining rapid T_2 -weighted images are severely compromised by rf power deposition (SAR) limitations, and substitution of T_2^* -weighted multi-slice gradient echo sequences would otherwise be contaminated by severe susceptibility artifacts. Finally, it should benefit microimaging of small objects at very high magnetic field strengths.

¹ Yang, Q.X., *et al.*, Proc. ISMRM, 4, 1993 (1997); 38th ENC (Orlando, FL), abstr. P-011 (1997).

² Yang, Q.X. *et al.*, J. Magn. Reson., 141(1), 1-6 (1999).

INSTRUMENTATION

Magnetic Properties of Various Metals for Pressure Cells

Jackson, D.D., NHMFL

Tozer, S., NHMFL

Cao, G., NHMFL

Crow, J.E., NHMFL

Fisk, Z., NHMFL

In the design of a pressure clamp, one of the important issues is determining the best material to use for the cell body. Not only is the strength of the material important, but its magnetic properties must be determined so that their effects on the measurements are well understood. MP35N is a steel whose mechanical properties are understood, but prior to this study, its behavior in magnetic fields was unclear. Our work at the NHMFL investigated the isothermal magnetization of MP35N at various temperatures (4.2 K, 80 K, 120 K, 295 K) up to 30 T using a vibrating sample magnetometer. It was found that even at the lowest temperatures studies, MP35N remains paramagnetic and never reaches saturation. The properties of the steel were studied on four samples: (1) as received from the manufacturer, (2) annealed in air, (3) annealed in air followed by mechanically removing an outer oxide layer, and (4) annealed in argon. It was found that the sample annealed in argon produced the best results for use in a pressure cell due to its low magnetization and simple, nearly linear form. The results of the various MP35N samples were also compared with that of a similar Russian Ni-Cr alloy, and various beryllium-copper samples. The isothermal magnetizations of all of the beryllium-copper samples were found to be at the limit of the background of the vibrating sample magnetometer. The results of these measurements will be useful in understanding the magnetic properties of the pressure clamps currently in design at the NHMFL.

^3He Melting Pressure Reduction in High Magnetic Field at Ultra-Low Temperatures

Xia, J. S., UF, Physics/NHMFL

Shvarts, V., UF, Physics/NHMFL

Adams, E.D., UF, Physics

We have constructed an experimental cell for the measurement of ^3He melting pressure depression with magnetic field up to 20 T to determine the magnetization of the ordered solid phases in the $T=0$ limit.

The cell is made out of brown Vespel and has ^3He and ^4He chamber with Capton membrane in between to enable solid phase growth with equilibrium polarization. A sapphire pressure transducer and Mylar thermometer, thermally anchored to the leads, are located inside the ^3He part of the cell. The main heat exchanger, with a total surface area of about 18 m², was fabricated from 9.2 g of Tokuriki ultra-fine silver powder compressed into a silver thermal link connected to the nuclear demagnetization stage.

Test experiments at temperatures down to 1 mK showed that both gauges have sufficient sensitivity of 0.3 pF/psi and 0.01 pF/mK, respectively, and do not display strong magnetic field dependence. Some pressure dependence of Mylar thermometer can be overcome by placing it in vacuum. Thermal contact in this case can be ensured by a large heat exchangers attached to the leads and placed into ^3He chamber.

We have used an Andeen-Hagerling 2500A automatic capacitance bridge for the capacitance thermometry, which gave us an accuracy of few μK with 0.1 V excitation and